NATIONAL ADVISORY COMMITTEE FOR AERONAUTICS

TECHNICAL NOTE 2706

EFFECT OF CHANGING PASSAGE CONFIGURATION ON INTERNAL-FLOW CHARACTERISTICS OF A 48-INCH CENTRIFUGAL COMPRESSOR

I - CHANGE IN BLADE SHAPE

By Donald J. Michel, John Mizisin, and Vasily D. Prian

Lewis Flight Propulsion Laboratory
Cleveland, Ohio

Washington
May 1952

NATIONAL ADVISORY COMMITTEE FOR AERONAUTICS

TECHNICAL NOTE 2706

EFFECT OF CHANGING PASSAGE CONFIGURATION ON INTERNAL-FLOW CHARACTERISTICS OF A 48-INCH CENTRIFUGAL COMPRESSOR

I - CHANGE IN BLADE SHAPE

By Donald J. Michel, John Mizisin, and Vasily D. Prian

SUMMARY

The passage contour of a 48-inch centrifugal impeller was modified by changing the shape of the blades with the objective of reducing the deceleration rates along the blade faces and thereby improving the internal efficiency of the impeller. A comparison of the internal-flow characteristics was made of the original and modified passage contours at the design flow rate. In addition, the internal-flow characteristics of the modified passage are presented and analyzed over the entire flow range from maximum flow to surge at a corrected impeller tip speed of 700 feet per second.

At design flow, the modified impeller, which had lesser deceleration rates along the blade surfaces, showed a general improvement in efficiency throughout the passage over that of the original impeller. It is concluded that impellers designed for prescribed velocity distributions with low rates of deceleration should have higher internal efficiencies than impellers with high rates of deceleration. At high weight flows (negative angles of attack), there were large separation losses at the inlet because of the shape of the leading edge; at low flow rates (positive angles of attack), the separation losses were not as great. The low-efficiency regions in the passage generally occurred near the flow surfaces with decelerating flow, except along the driving face where most boundary-layer build-up by adverse velocity gradients was probably eliminated by secondary flows or bleeding through the clearance space.

INTRODUCTION

The flow characteristics within the rotating passages of a large radial-inlet centrifugal impeller have been determined experimentally at the NACA Lewis laboratory (references 1 and 2). Along the trailing

face, a low-efficiency region generally occurred as a result of a shift of low-energy air toward the trailing face and losses caused by the deceleration of air. By changing the passage area and the contour of the blades, the velocity distribution was adjusted to give smaller decelerations along the trailing face; better flow characteristics throughout the passage resulted.

In the first phase of this program, the area of the passage was changed by modification of the blade thickness. This modification was accomplished by gluing balsa wood of the desired shape to the driving surface of the impeller blades (references 1 and 2). The investigation reported herein, was concerned solely with the improvement of internal efficiency in the region of the impeller in which the velocities were controlled. No improvement in over-all efficiency was expected because the blunt tips of the modified blade caused increased mixing losses in the vaneless diffuser, thus cancelling the effects of improved flow characteristics in the impeller passages. The modified compressor was operated over the flow range from maximum flow to surge at a corrected tip speed of 700 feet per second. Experimental and theoretical pressures, velocities, and efficiencies were computed for the modified impeller and the flow characteristics of the modified and the original impellers at design flow are compared herein. Experimental results of flow conditions within the modified passage over the entire flow range investigated are presented.

APPARATUS

The modified impeller used in this investigation is shown in figure 1. The blade-thickness modification was determined by prescribing a velocity distribution along the blade surfaces, using a trial-and-error method of determining thickness, and then analyzing the resultant velocity distribution by the method of reference 3 until the required blade shape was evolved. The blades were modified by gluing balsa wood to the driving face of the original aluminum blade; the trailing-face contour and the blade height were left unchanged. A comparison of the original and the modified blade shapes is presented in figure 2. The pertinent blade data for the modified impeller are presented in table I. The blade thickness was so corrected that the actual passage area at any radius could be computed from the blade height without consideration of blade taper.

The over-all compressor and the impeller instrumentation are described in references 1 and 2. Some total-pressure probes and static-pressure taps near the driving face at the outer radii were covered by the balsa; they therefore were not used. Also, the blade-surface static pressures could not be read on this impeller. A schematic diagram of the location of the instruments is shown in figure 3. The total pressure

was measured by Keil type probes, set at the mean height of the blade for any given radius. The static pressure was measured through 0.030-inch-diameter orifices in the impeller hub. The pressure-transfer device was of the sealed ball bearing type. The instruments and the pressure-transfer device are fully described in reference 1.

PROCEDURE

The compressor was operated over the full flow range from a maximum corrected weight flow $W\sqrt{\theta}/\delta$ of 41 pounds per second to surge at 10 pounds per second, at a corrected tip speed $U/\sqrt{\theta}$ of 700 feet per second. (All symbols are defined in the appendix.) The operating procedure is described in reference 1.

The theoretical pressures and velocities were computed by the methods given in reference 3. The experimental velocities and efficiencies were computed by the method given in reference 2.

In addition to the usual experimental error in measurement, the pressures measured in the impeller could have a small consistent error due to the correction for the centrifugal force effect on the pressure column (reference 1). In the determination of velocity (a function of local total- to static-pressure ratio) at any point within the impeller, the quantity is primarily dependent upon the expression $\left[\left(\frac{P}{p}\right)^{\frac{\gamma-1}{\gamma}} - 1.0\right]$. When the pressure ratio P/p is close to 1.0, the expression involves small differences of large numbers and a small error in the measured pressure would give a large error in velocity. However, when the pressure ratio is high, the possible error is small. Thus, because the velocity in the passage was in general increased by the modified blade shape, the error in the velocity measurement would be somewhat less at the outer radii of the modified blades than on the original blades. Likewise, if because of experimental error, the local total pressure is slightly greater than the ideal value, the computed local efficiency could be considerably greater than 1.0.

RESULTS AND DISCUSSION

Over-All Performance

Although the primary purpose of this report is to study the effect of modifying the blade shape on the internal-flow characteristics of the impeller, the over-all performance is presented briefly for the sake of completeness. A comparison of the over-all performance of the original and the modified compressors is shown in figures 4 and 5. Although the

over-all adiabatic efficiencies were about the same for both impellers, the total-pressure ratio of the modified impeller was less because the slip factor was less. The peak total-pressure ratio dropped from 1.455 in the original impeller to about 1.375 in the modified impeller with an accompanying drop in slip factor from 0.89 to 0.78. The weight-flow range changed from 44 to 14 pounds per second for the original configuration to a range of 41 to 10 pounds per second for the modified impeller.

Comparison of Internal-Flow Characteristics of Original and Modified Impellers at Design Flow Rate

A comparison of the internal-flow characteristics for the original and the modified impeller passages at the design weight flow, 26 pounds per second, is presented in figure 6. The theoretical static pressures along the blade faces (fig. 6(a)) are similar for both passages except near the tip where the effect of the slip factor closes the pattern, thereby indicating that less work is done on the air in the modified impeller than in the original impeller. The modified blades unload at about the 23-inch radius because of the sharp cut-back of the blade at that point.

The total-pressure distribution near the driving face of the blade (fig. 6(b)) shows little difference between the original and the modified blades except near the tip where the modified blade is cut-back. Both show isentropic flow over almost the entire blade length. On the trailing face, however, the pressure ratio for the modified blade was almost isentropic over nearly the entire blade length whereas, for the original blade, the pressure was lower after the 14-inch radius. The fact that the pressure appears to be greater than isentropic may be due to experimental error in the pressure measurement which, as previously mentioned, would make the pressures consistently high.

The relative adiabatic efficiency, which is a function of the relative total pressure (reference 1), is shown in figure 6(c) by lines of constant efficiency throughout the passage. Because of the possible error in pressure measurement, efficiencies over 1.0 were computed. However, none of the efficiency contours over 1.0 are shown; the line of $\eta_{ad} = 1.0$ indicates the limit of isentropic flow. The greatest errors in efficiency occur in the inlet region where the pressure rise is very small. However, even though the absolute value of the efficiency may be in error, it is believed that qualitative comparisons of inlet-efficiency contours can be made between impellers and over the flow range. There was a general improvement in efficiency in the passage as shown by the much larger area in which $\eta_{ad} = 1.0$, and by the fact that the minimum passage efficiency was higher than that of the original passage. There were no losses at the inlet or along the faces except

near the tip; the original impeller showed a drop in efficiency all along the trailing face. In the modified passage, the lower efficiency region starts at about the 16-inch radius near the trailing face and spreads toward the passage center at the tip. Discounting the portion of the passage beyond where the blade is cut-back, (radii greater than approximately 23 in.), a low-efficiency region in which $\eta_{ad} = 0.875$ is reached near the center of the passage. With the original passage, a low-efficiency region in which $\eta_{ad} = 0.80$ was found near the trailing face.

The velocity contours throughout the passages and near the blade faces are shown in figures 6(d) and 6(e). The velocity is almost constant along the trailing face for the modified passage whereas, for the original passage, the velocity decelerates from the 14-inch radius to the tip. Because the velocity gradient along the trailing face of the modified passage is not conducive to boundary-layer build-up, the losses along that face are minimized, and good efficiency results. As pointed out in reference 2, the large deceleration along the driving face does not result in an efficiency drop, probably because the boundary layer is thin on the driving face near the inlet and therefore can sustain a greater deceleration and also because secondary flows or bleeding through the clearance space between the blade and shroud removes any boundary-layer build-up. The velocity along the driving face agreed in trend with that theoretically predicted but was higher over the blade length (fig. 6(e)). On the trailing face, the velocity at the inlet was slightly lower than that predicted and deceleration occurred from the 18-inch radius to the tip at about the same rate as was predicted by theory.

From the foregoing comparison, it is concluded that impellers designed for prescribed velocity distributions with low rates of deceleration should have higher internal efficiencies than impellers with high rates of deceleration.

Variation in Internal-Flow Characteristics of Modified Impeller with Flow Rate

The efficiency distribution throughout the modified impeller passage and the experimental velocity contours over a range of corrected weight-flow rates are shown in figures 7 and 8. The efficiency contours (fig. 7) indicate that regions of large loss occur in the vicinity of the leading edge and along the flow surfaces with high rates of deceleration. In addition, there is evidence of secondary flows that replace high-energy air with low-energy air. These phenomena are discussed in the following paragraphs.

At high flow rates (figs. 7(a) to 7(d)) a low-efficiency region exists on the driving face near the inlet. This region exists because of flow separation due to the negative angle of attack (stagnation point on the trailing face). For the maximum flow rate this angle of attack is maximum and the separation losses are maximum as indicated by the large region of low efficiency. As the flow rate decreases, the separation losses decrease, and the region of low efficiency reduces. At the design angle of attack (fig. 7(e)), separation losses at the inlet were not apparent.

As the flow rate decreases below the design value, the angle of attack becomes positive (stagnation point on the driving face) and separation occurs on the trailing face at the inlet (figs. 7(f) to 7(i)). As this separation becomes progressively greater with decreasing flow rate, the internal efficiency becomes progressively lower. However, for the low flow rates (positive angles of attack), the separation losses, indicated by the efficiency contours, are not as great as for the high flow rates (negative angles of attack); this is further indicated in figure 9 where the distribution of total pressure along the blade surfaces is given for three flow rates. At maximum flow (large negative angle of attack), $W\sqrt{\theta}/\delta = 41$ pounds per second, the large pressure drop at the inlet is caused by the separation of the flow around the leading edge of the blade. At design flow (0° angle of attack), $W\sqrt{\theta}/\delta = 26$ pounds per second, a continuous rise in pressure, which was nearly isentropic for both faces, occurred. At a large positive angle of attack, $W\sqrt{\theta}/\delta = 12.5$ pounds per second, there was no pressure drop along the trailing face, but the pressure did not begin to rise until the 14-inch radius. Because of the shape of the leading edge of the blade (fig. 2), separation from the driving face at negative angles of attack (high flow rates) should be more serious than separation from the trailing face at positive angles of attack (low flow rates); because of this effect and the greater losses at high weight flows, as discussed in reference 4, the over-all efficiency might be expected to decrease more sharply at the high flow rates than at the low flow rates, as indicated in figure 5.

The low-efficiency regions generally occur in the area where the flow decelerates along the flow surface except along the driving face inlet as previously discussed. At the high flow rates, because acceleration occurs over most of the trailing face length, there are few losses; if the losses do not increase as energy is added to the fluid as it moves radially outward, there is an apparent increase in relative efficiency (reference 2). As the flow rate decreases, the deceleration along the trailing face starts earlier (figs. 8(f) to 8(i)) and the efficiency starts to drop in that same region (figs. 7(f) to 7(i)).

Some evidence of secondary flows is seen in figure 7. In particular, the increase in efficiency to 1.00 along the trailing face at the high flow rates (figs. 7(a) to 7(c)) is impossible in the two-dimensional case

unless there is a shift of higher energy air into the plane of measurement; thus, there must be a shift of higher energy air at the trailing-face tip region by some secondary flow process at these high weight flows. At the lower weight flows (figs. 7(f) to 7(i)), the passage of the fluid through the impeller is sufficiently slow to allow a shift of low-energy air from the driving face toward the trailing face of the next blade as noted and discussed in reference 2.

There were regions of reversed flow at the trailing-face tip at the lower flow rates (figs. 8(g) and 8(h)) apparently caused by the blade cut-back. At the 12.5-pound-per-second flow rate, there was a region of reversed flow near the trailing face starting at about the 16-inch radius. The losses associated with these flow reversals were apparently not too great as there was not a large drop in efficiency in those regions, although they were the lowest-efficiency regions in the passage. At the surge condition ($W\sqrt{\theta}/\delta$ = 10 lb/sec), the efficiency never reached 1.0 in the passage or at the inlet (fig. 7(i)), probably because of the unstable nature of the flow due to recirculation in the passage at the surge condition.

RESULTS AND CONCLUSIONS

The following results were obtained in an investigation of a 48-inch centrifugal impeller that was modified by changing the shape of the blades:

1. At design flow, the deceleration rates were lower along the flow surfaces in the modified impeller and there was a general improvement in the efficiency throughout the passage over that which existed in the original impeller. It is concluded that impellers designed for prescribed velocity distributions with low rates of deceleration should have higher internal efficiencies than impellers with high rates of deceleration.

2. At high weight flows (negative angle of attack), there were large separation losses at the inlet whereas at low weight flows (positive angle of attack) the separation losses were not as great because of the shape of the leading edge.

3. Over the flow range, lower efficiency regions generally occurred near the flow surfaces with decelerating flow, except along the driving face where most boundary-layer build-up by adverse velocity gradients was probably eliminated by secondary flows or bleeding through the clearance space.

Lewis Flight Propulsion Laboratory
National Advisory Committee for Aeronautics
Cleveland, Ohio

APPENDIX - SYMBOLS

The following symbols are used in this report:

c_0 stagnation speed of sound upstream of impeller, ft/sec

P total pressure

p static pressure

q stream velocity, ft/sec

r radius, in.

U impeller tip speed, ft/sec

W weight flow, lb/sec

γ ratio of specific heats

δ ratio of actual inlet total pressure to standard sea-level pressure

η_{ad} adiabatic efficiency

θ ratio of actual inlet total temperature to standard sea-level temperature

Subscripts:

0 inlet measuring station

2 diffuser measuring station

r relative to impeller

REFERENCES

1. Michel, Donald J., Ginsburg, Ambrose, and Mizisin, John: Experimental Investigation of Flow in the Rotating Passages of a 48-Inch Impeller at Low Tip Speeds. NACA RM E51D20, 1951.

2. Prian, Vasily D., and Michel, Donald J.: An Analysis of Flow in Rotating Passage of Large Radial-Inlet Centrifugal Compressor at Tip Speed of 700 Feet per Second. NACA TN 2584, 1951.

3. Stanitz, John D., and Prian, Vasily D.: A Rapid Approximate Method for Determining Velocity Distribution on Impeller Blades of Centrifugal Compressors. NACA TN 2421, 1951.

4. Lieblein, Seymour: Theoretical and Experimental Analysis of One-Dimensional Compressible Flow in a Rotating Radial-Inlet Impeller Channel. NACA TN 2691, 1952.

TABLE I - BLADE DATA AT MEAN HEIGHT

Radius (in.)	Blade angle (deg)		Total blade height (in.)	Thickness (in.)	
	Driving face	Trailing face		Actual	Corrected
12.3	-57.7	-57.7	3.30	0.730	0.897
13.0	-55.3	-55.3	3.05	.714	.873
14.0	-50.9	-50.9	2.72	.665	.817
16.0	-26.0	-32.5	2.23	.821	.896
18.0	-8.2	-16.7	1.91	1.328	1.401
20.0	0	-3.0	1.69	1.641	1.731
21.5	8.5	0	1.53	1.953	1.991
22.5	12.0	0	1.45	2.109	2.139
23.5	-51.0	-4.4	1.40	1.953	1.993

Figure 1. - Impeller used in investigation of flow within rotating passages.

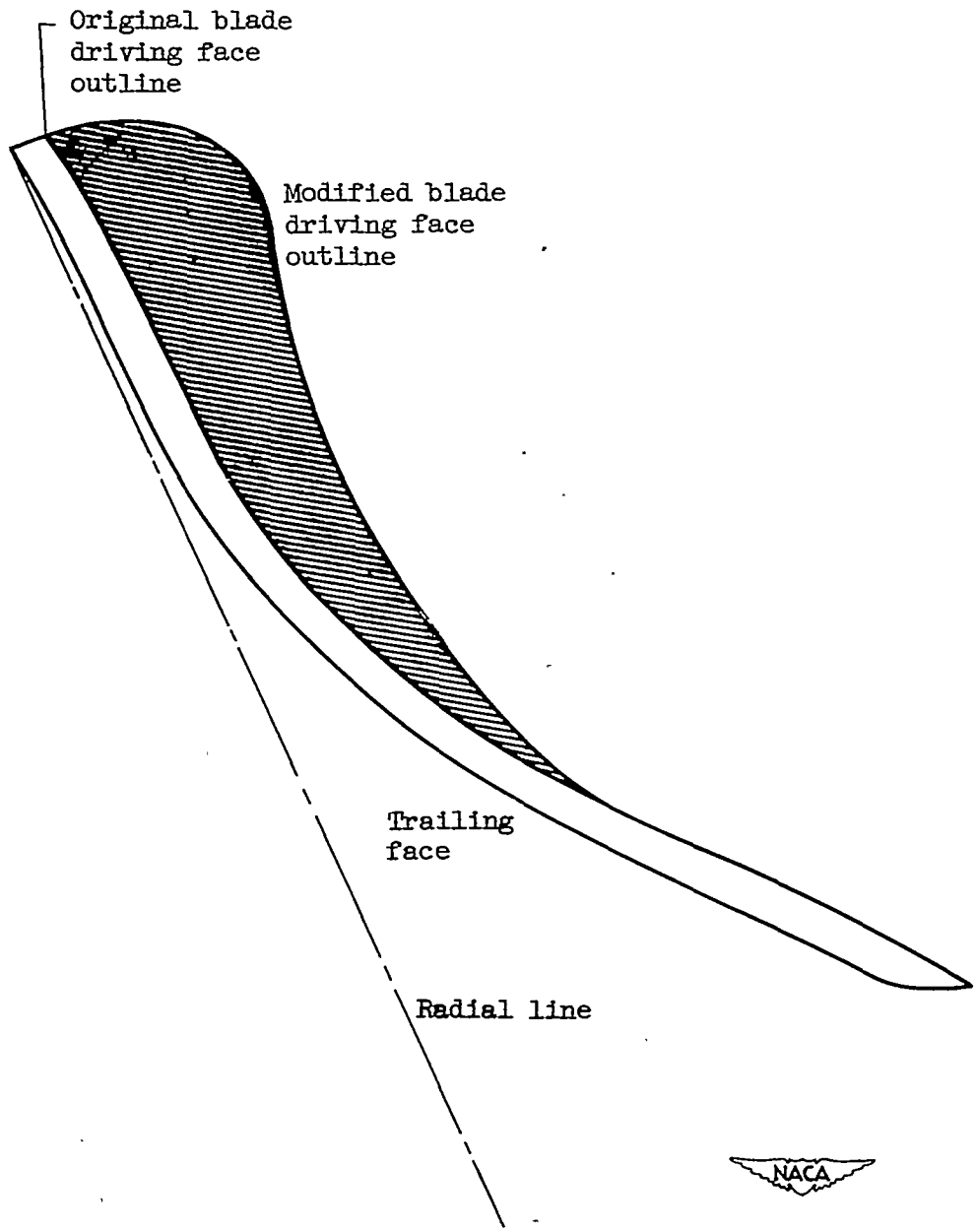

2530

Figure 2. - Comparison of original and modified blade shapes.

2530

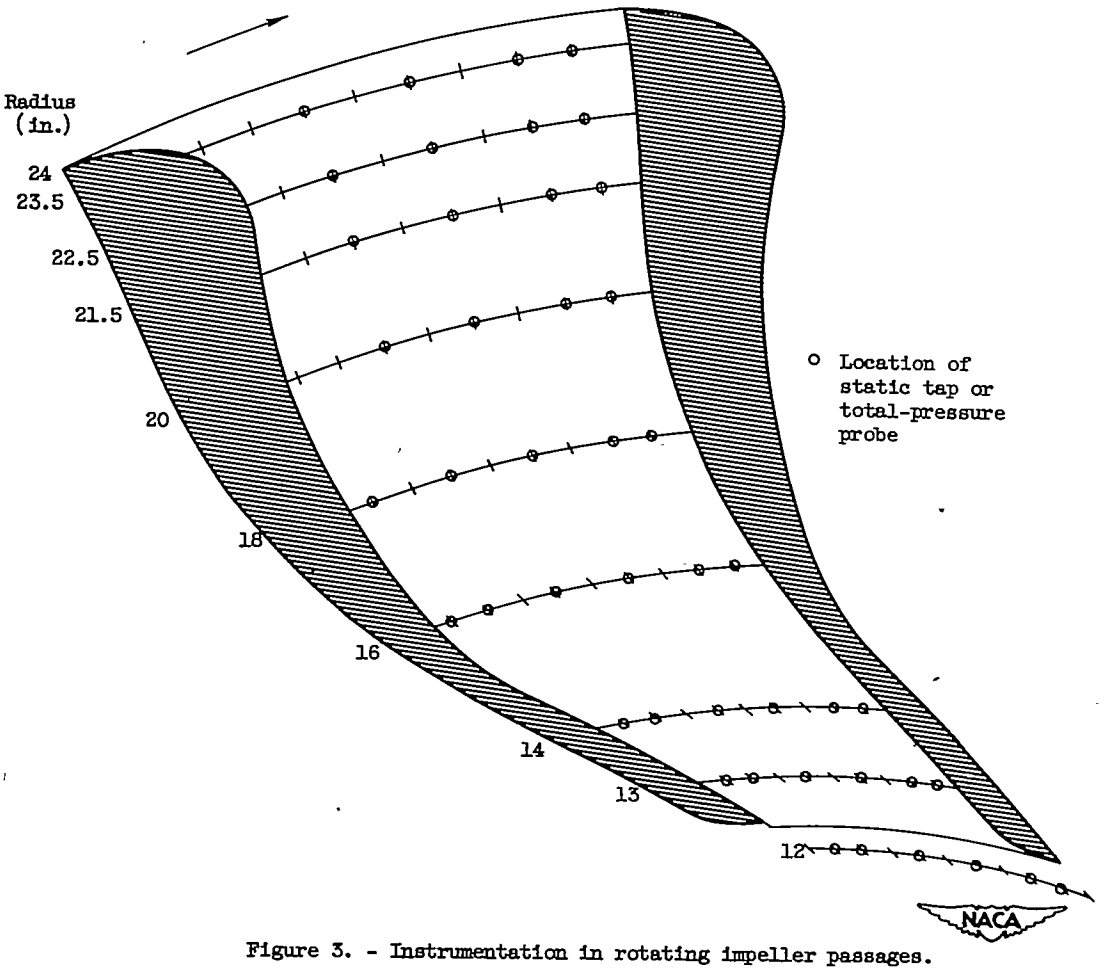

Figure 3. - Instrumentation in rotating impeller passages.

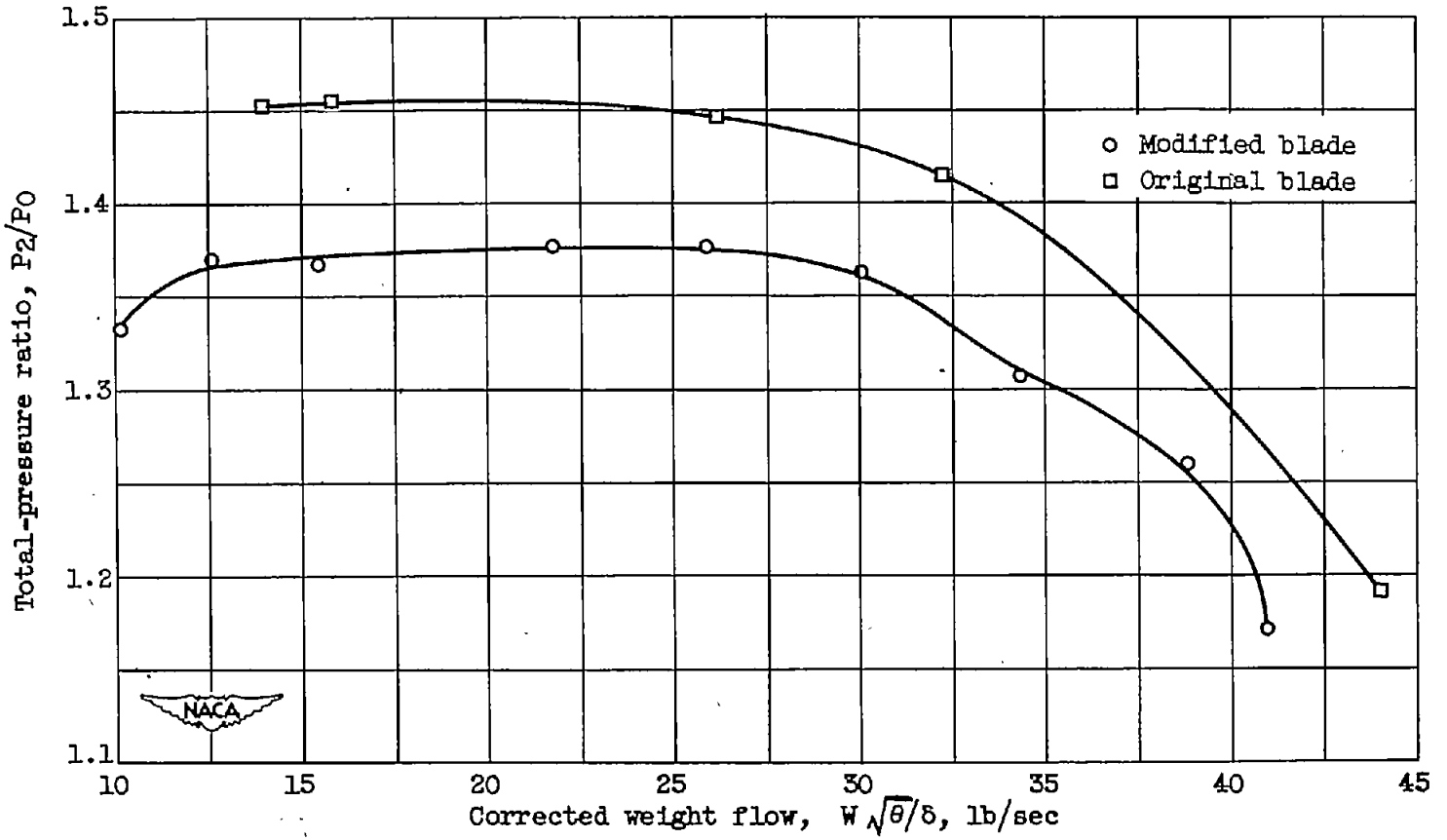

Figure 4. - Pressure rise through impeller based on conditions at diffuser tip $\left(1\frac{1}{2}\right.$ impeller rad$\left.\right)$ for original and modified blades. Corrected tip speed, 700 feet per second.

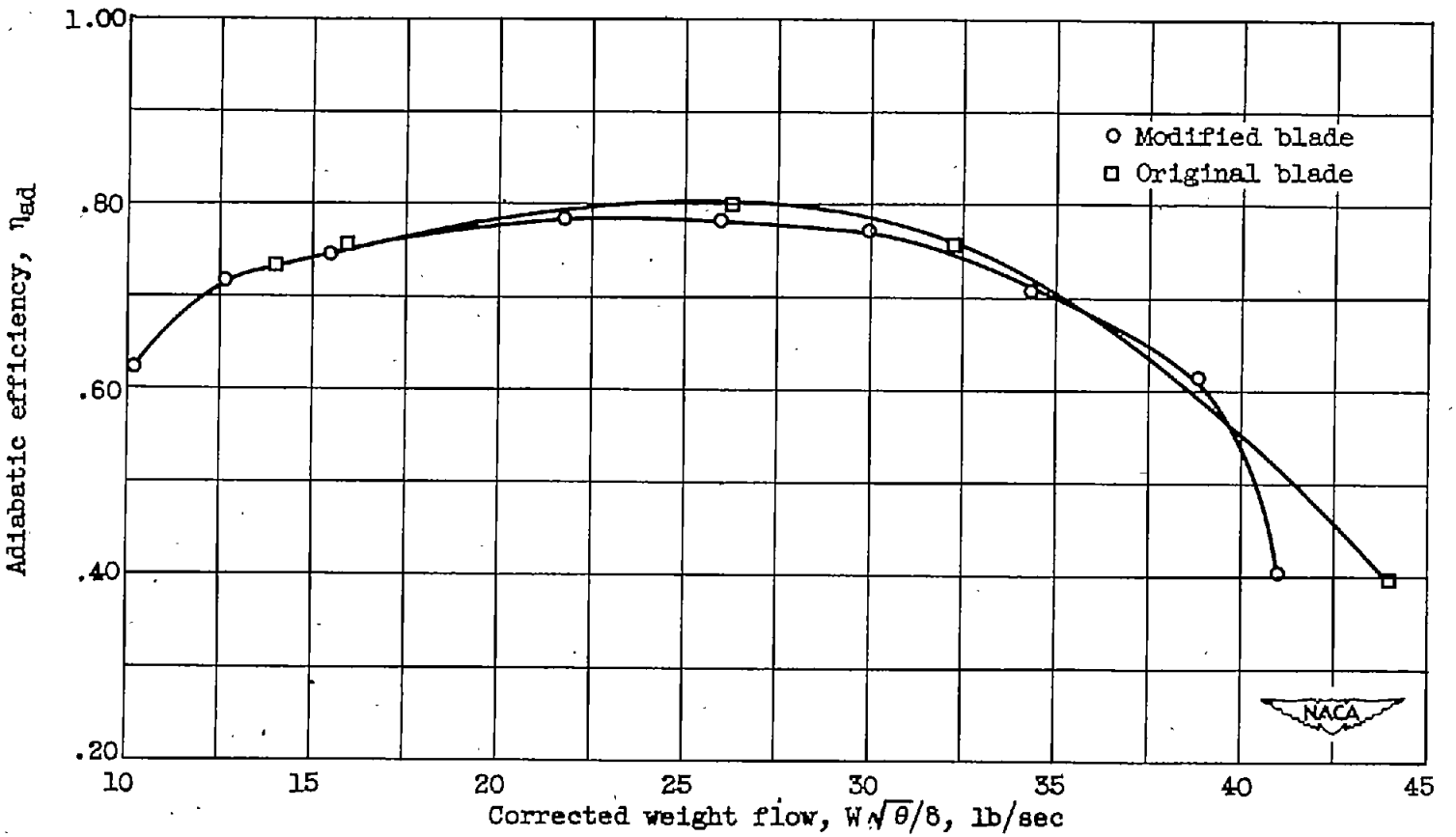

Figure 5. - Adiabatic efficiency of impeller and diffuser based on conditions at diffuser tip $\left(1\frac{1}{2}\right.$ impeller rad$\left.\right)$ for original and modified blades. Corrected tip speed, 700 feet per second.

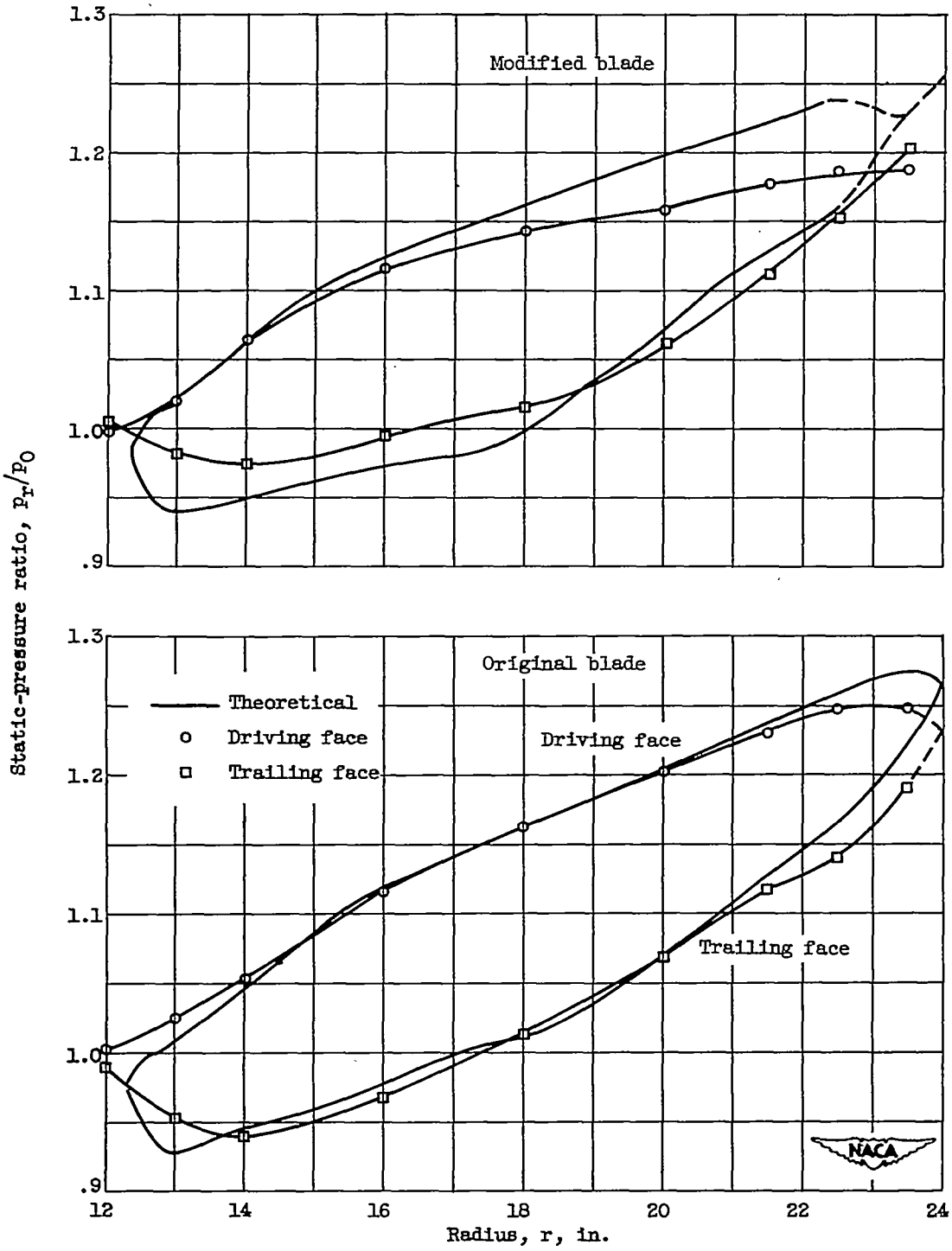

(a) Static-pressure distribution along blade faces.

Figure 6. - Flow characteristics in impeller rotating passage at corrected weight flow of 26 pounds per second.

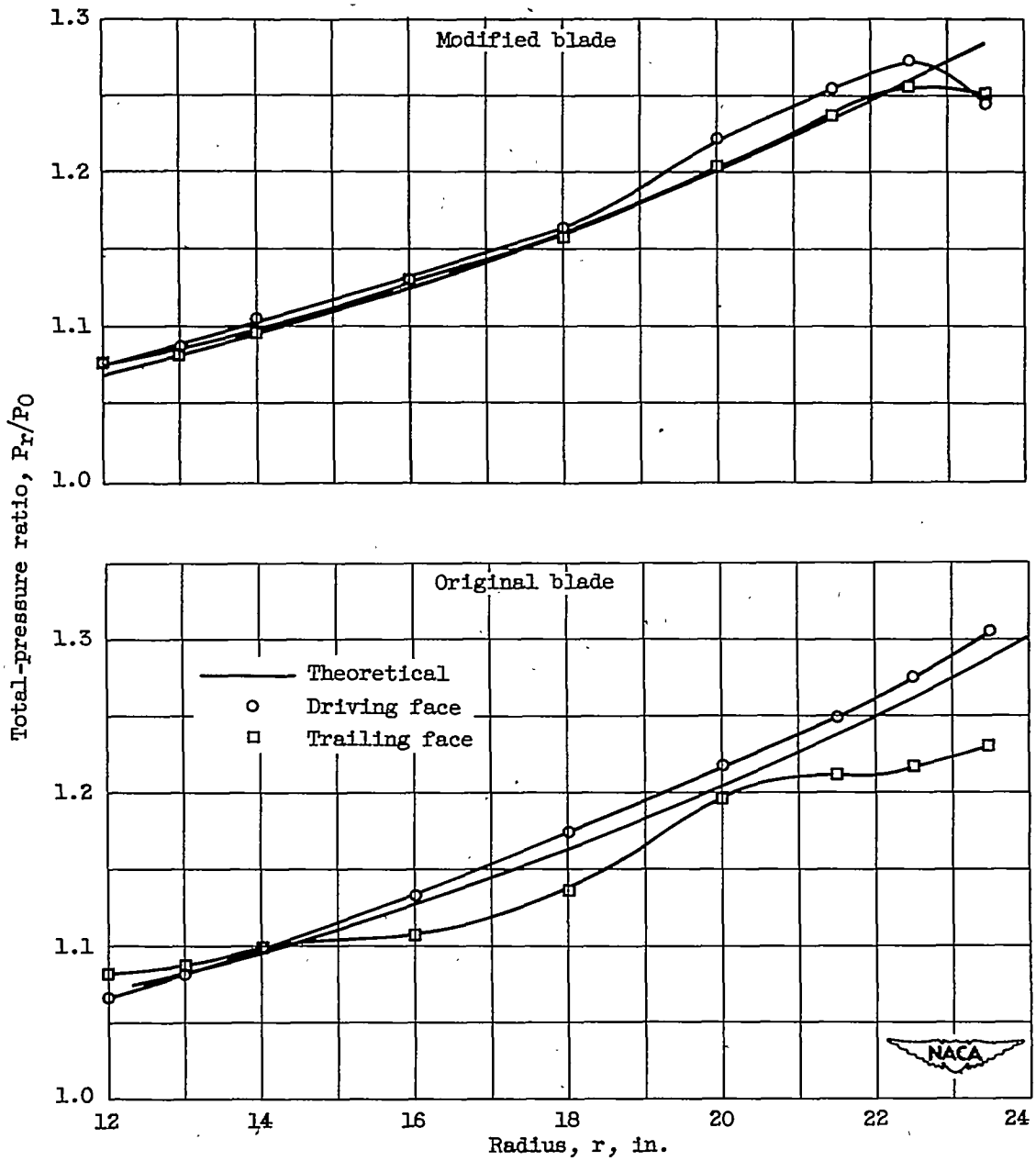

(b) Total-pressure distribution along blade faces.

Figure 6. - Continued. Flow characteristics in impeller rotating passage at corrected weight flow of 26 pounds per second.

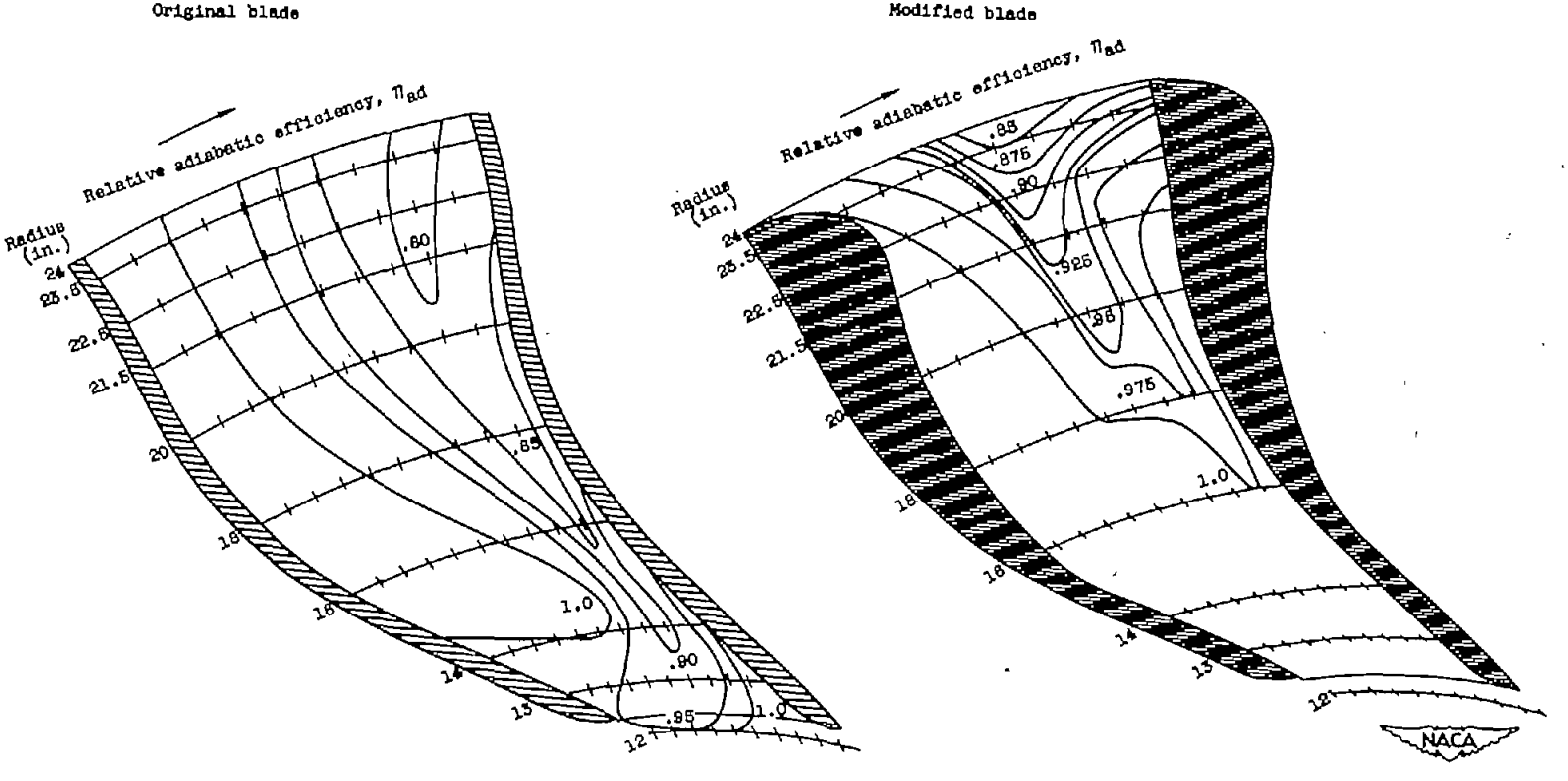

(c) Relative adiabatic efficiency distribution throughout passage.

Figure 6. - Continued. Flow characteristics in impeller rotating passage at corrected weight flow of 28 pounds per second.

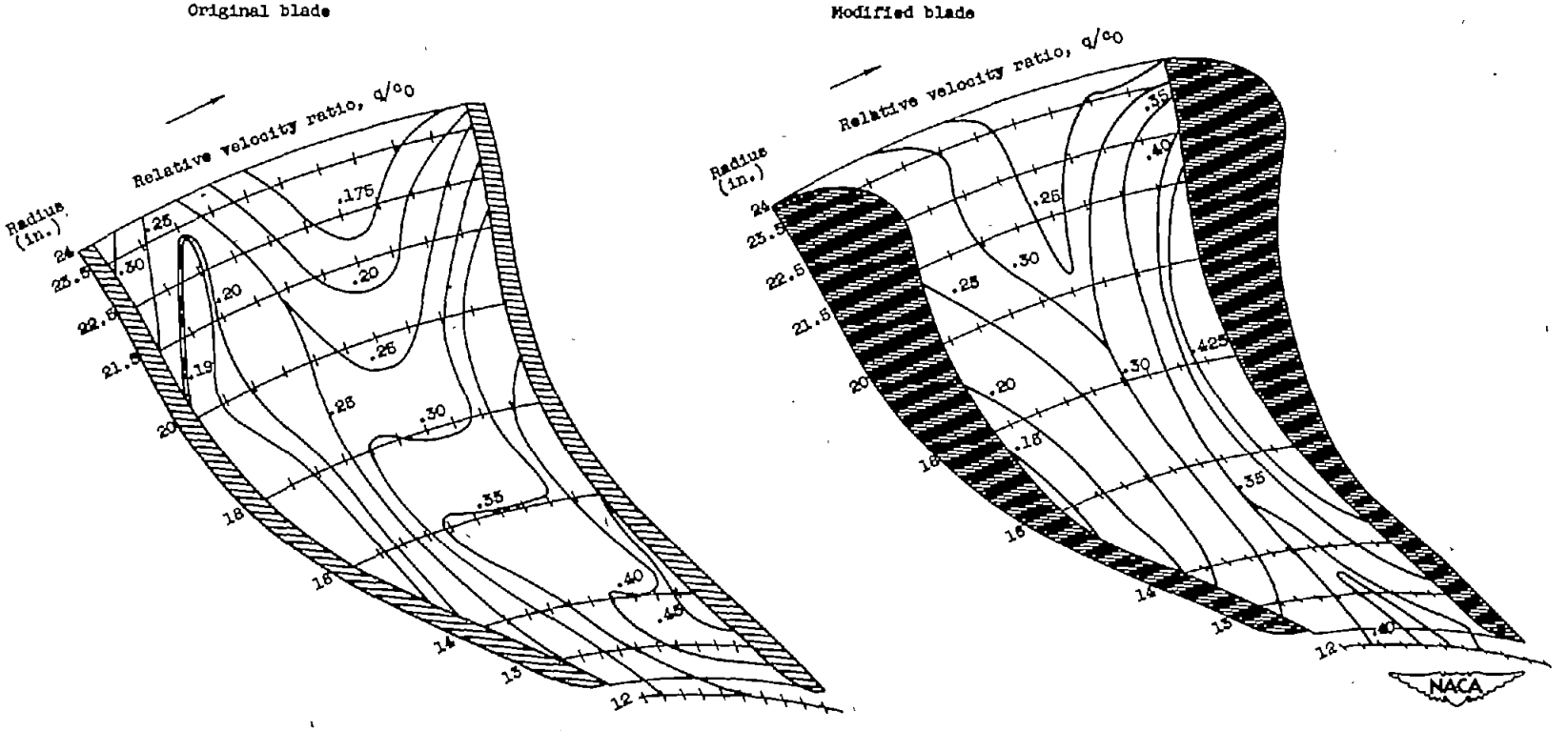

(d) Velocity distribution throughout passage.

Figure 8. - Continued. Flow characteristics in impeller rotating passage at corrected weight flow of 26 pounds per second.

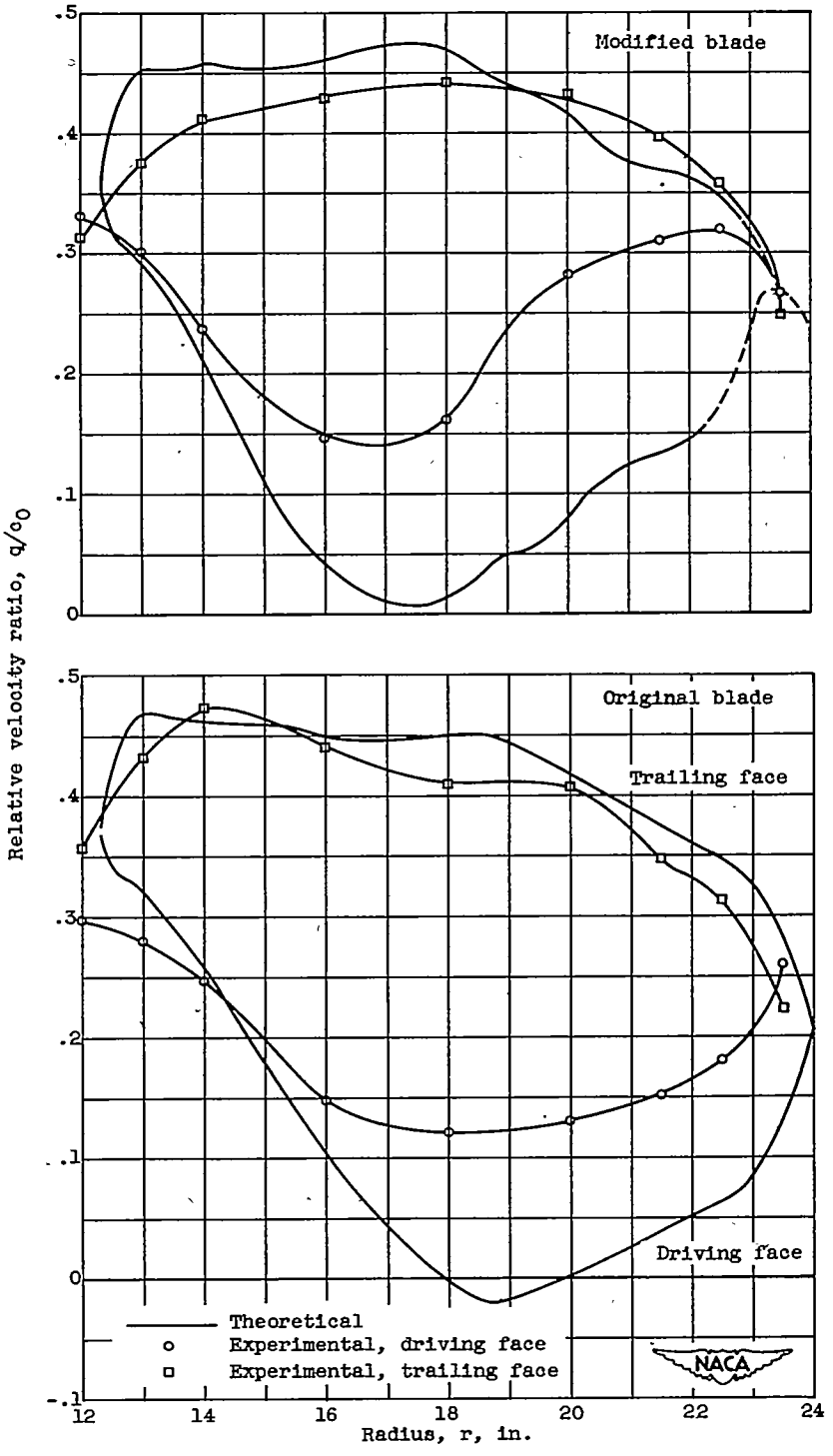

(e) Velocity distribution along blade faces.

Figure 6. - Concluded. Flow characteristics in impeller rotating passage at corrected weight flow of 26 pounds per second.

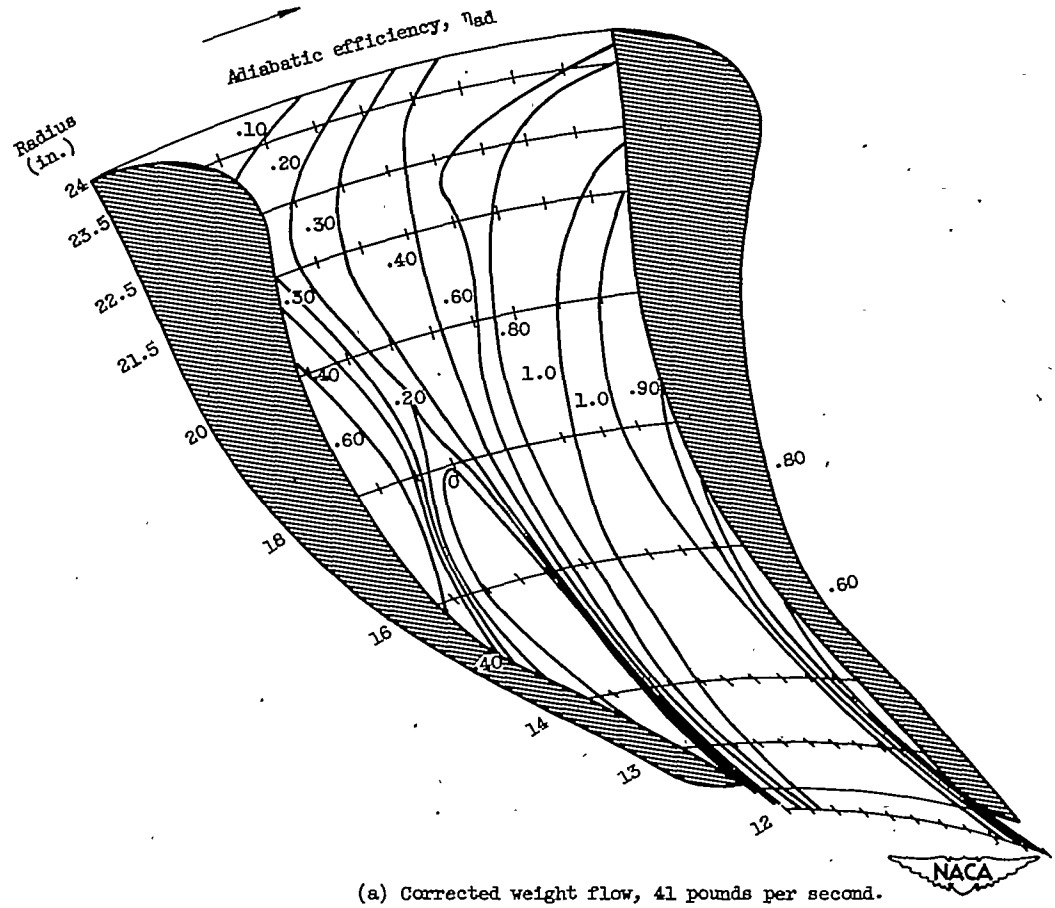

(a) Corrected weight flow, 41 pounds per second.

Figure 7. - Distribution of relative adiabatic efficiency throughout modified impeller passage.

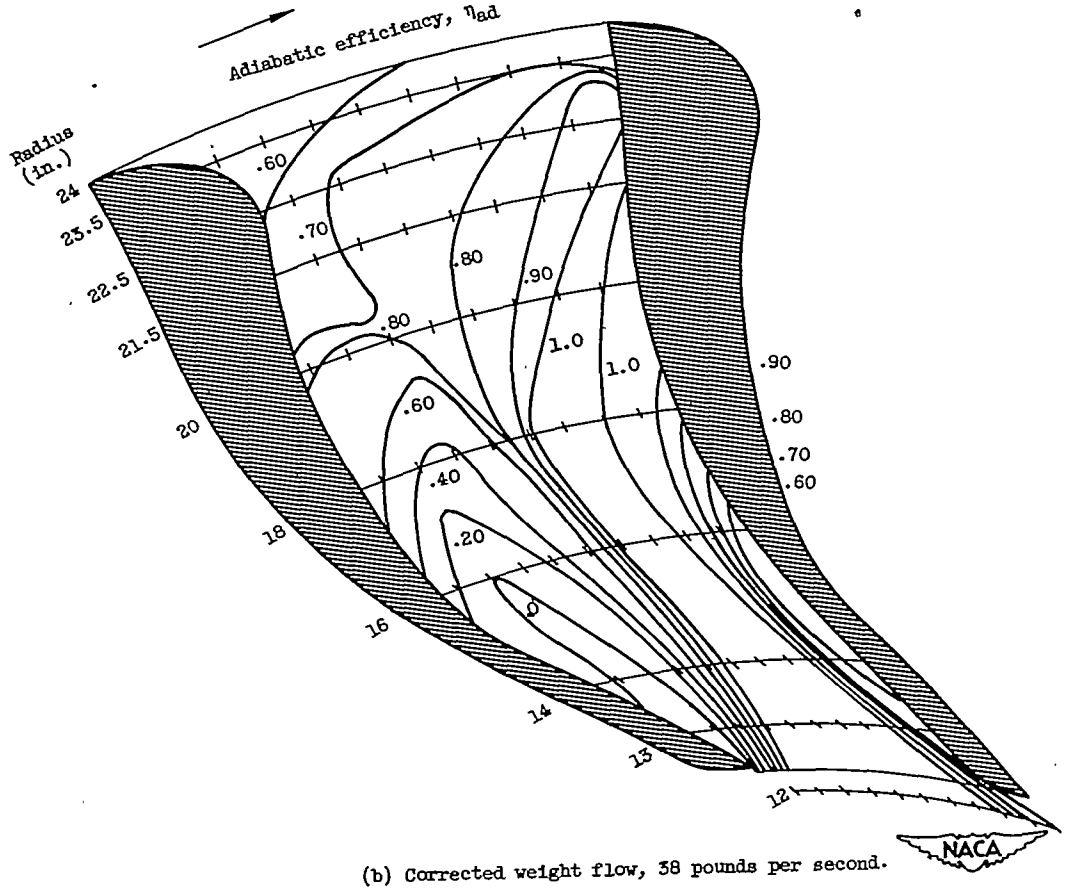

(b) Corrected weight flow, 38 pounds per second.

Figure 7. - Continued. Distribution of relative adiabatic efficiency throughout modified impeller passage.

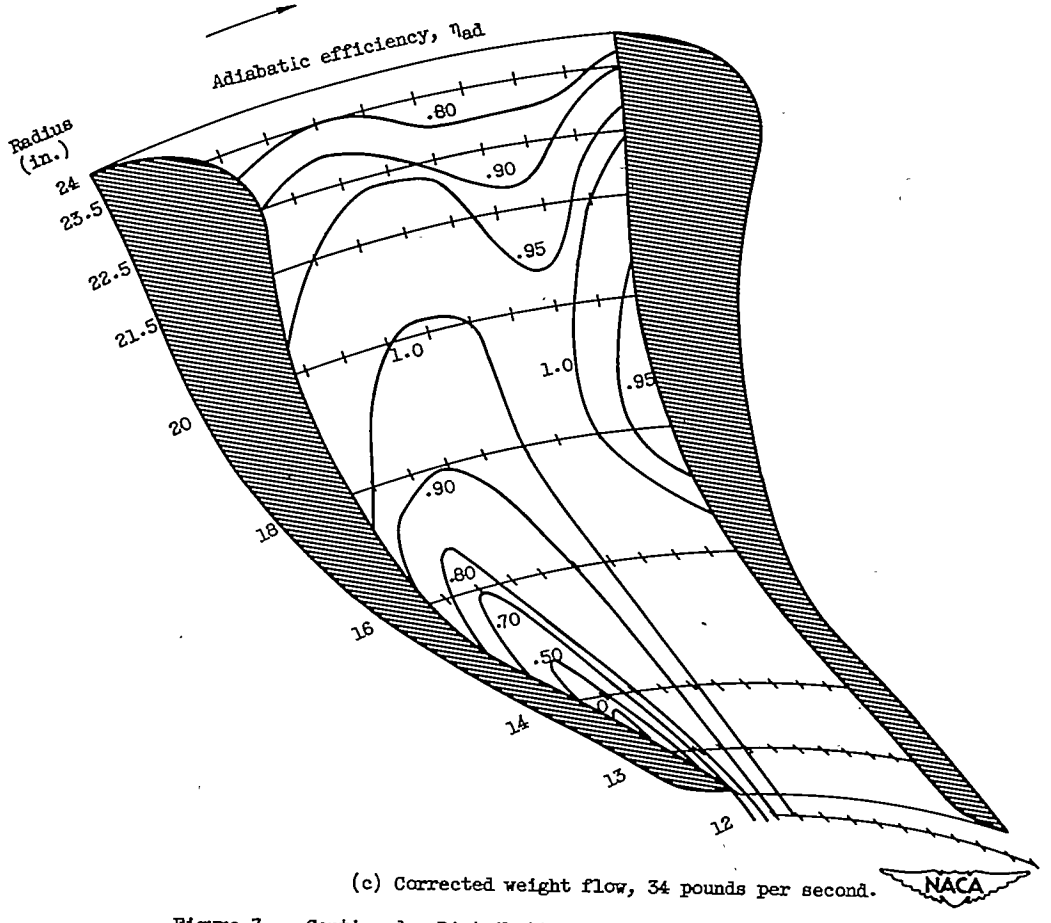

(c) Corrected weight flow, 34 pounds per second.

Figure 7. - Continued. Distribution of relative adiabatic efficiency throughout modified impeller passage.

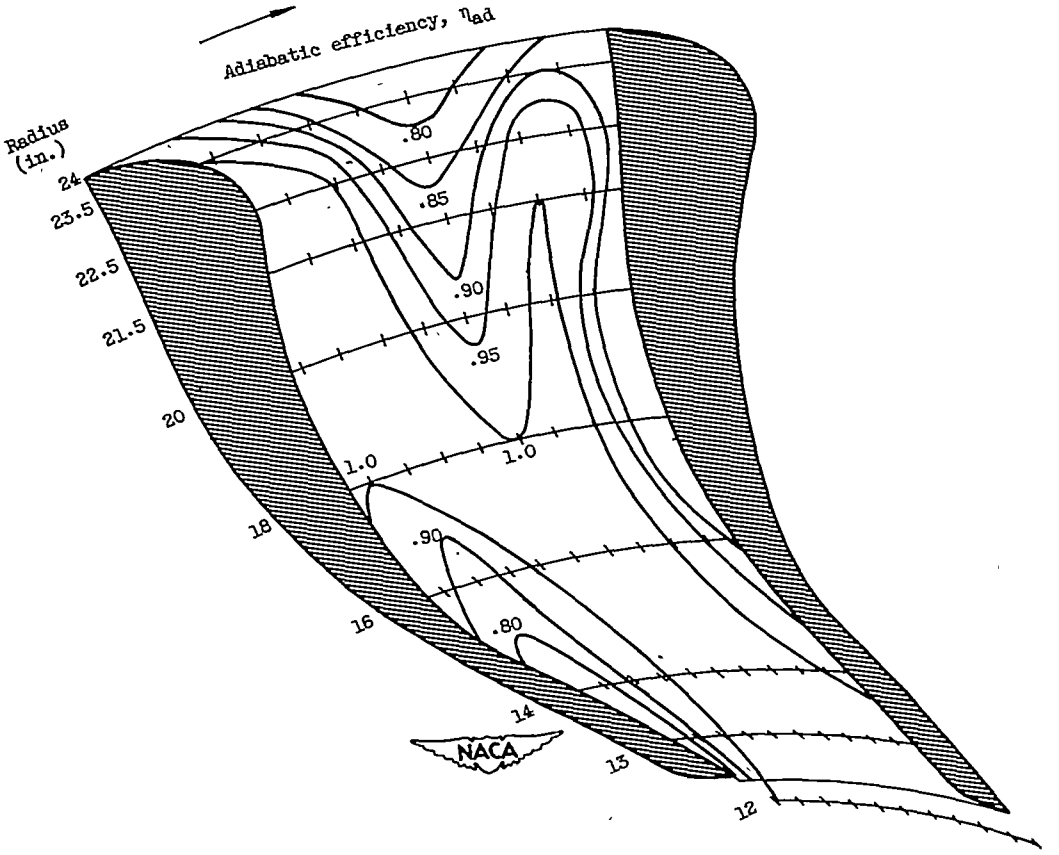

(d) Corrected weight flow, 30 pounds per second.

Figure 7. - Continued. Distribution of relative adiabatic efficiency throughout modified impeller passage.

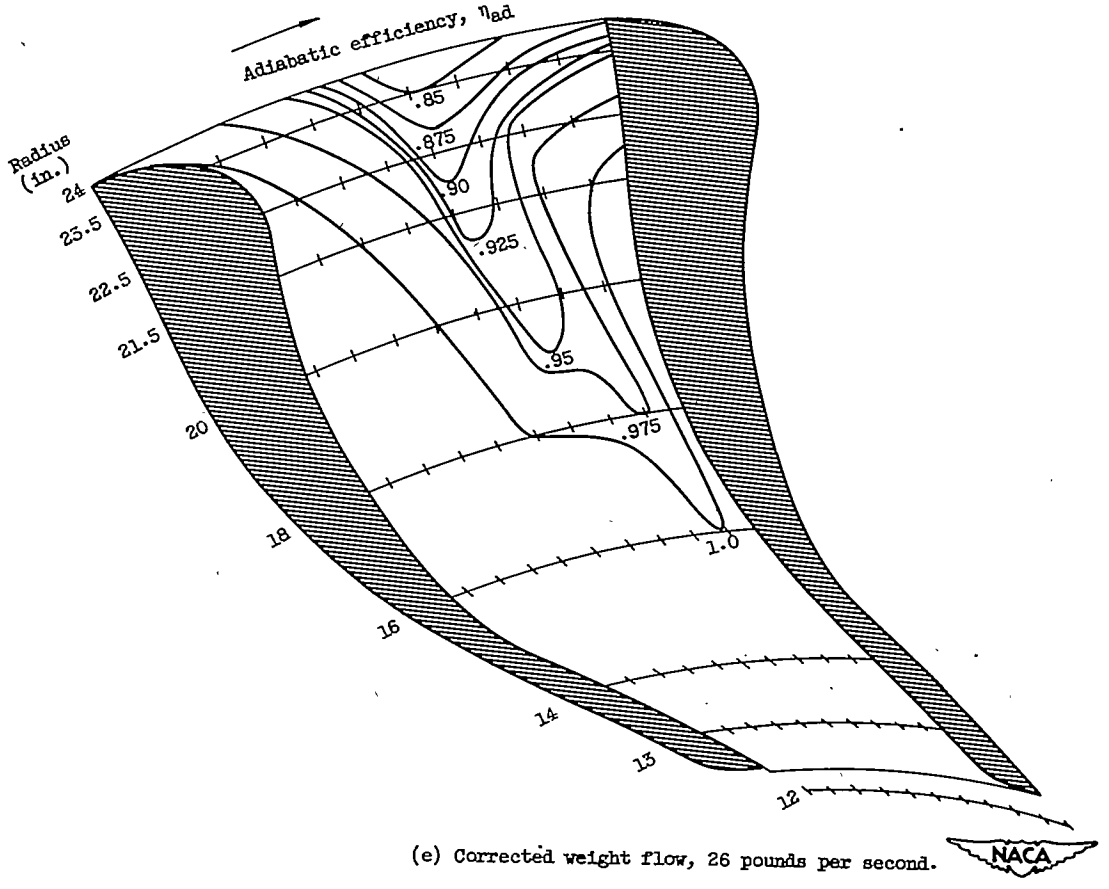

(e) Corrected weight flow, 26 pounds per second.

Figure 7. - Continued. Distribution of relative adiabatic efficiency throughout modified impeller passage.

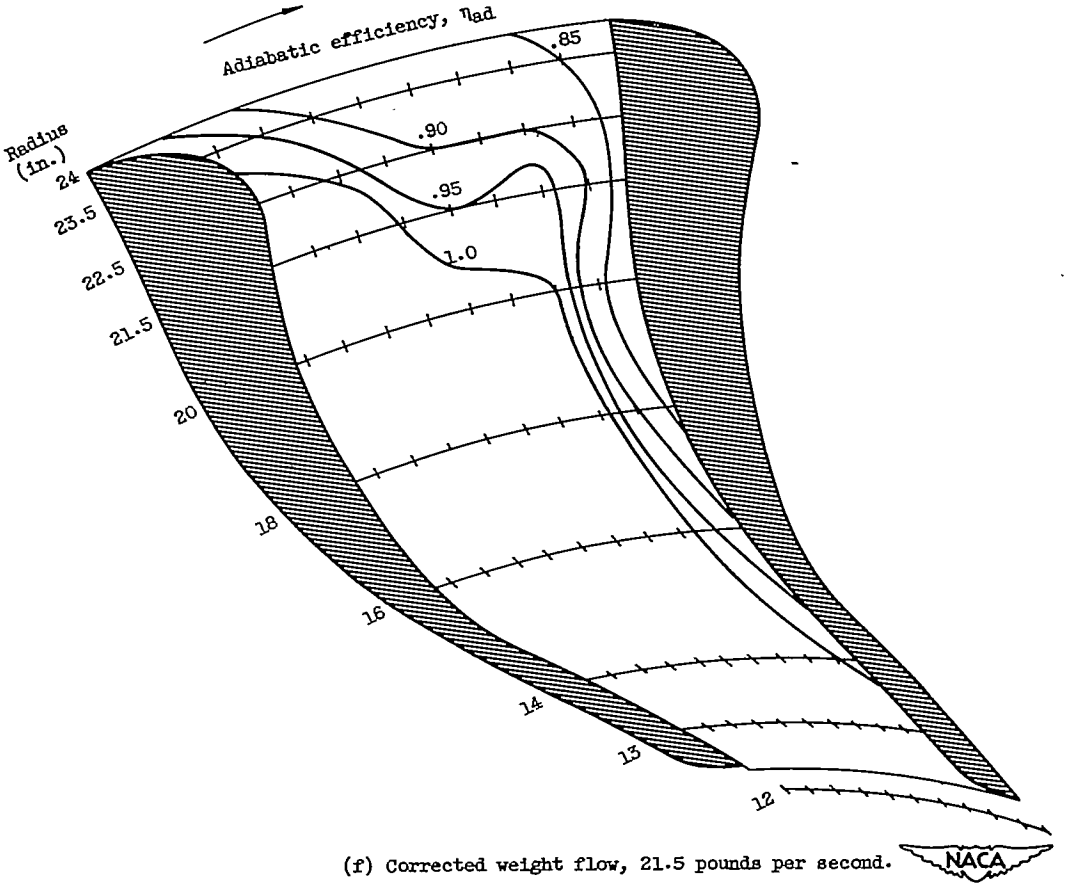

(f) Corrected weight flow, 21.5 pounds per second.

Figure 7. - Continued. Distribution of relative adiabatic efficiency throughout modified impeller passage.

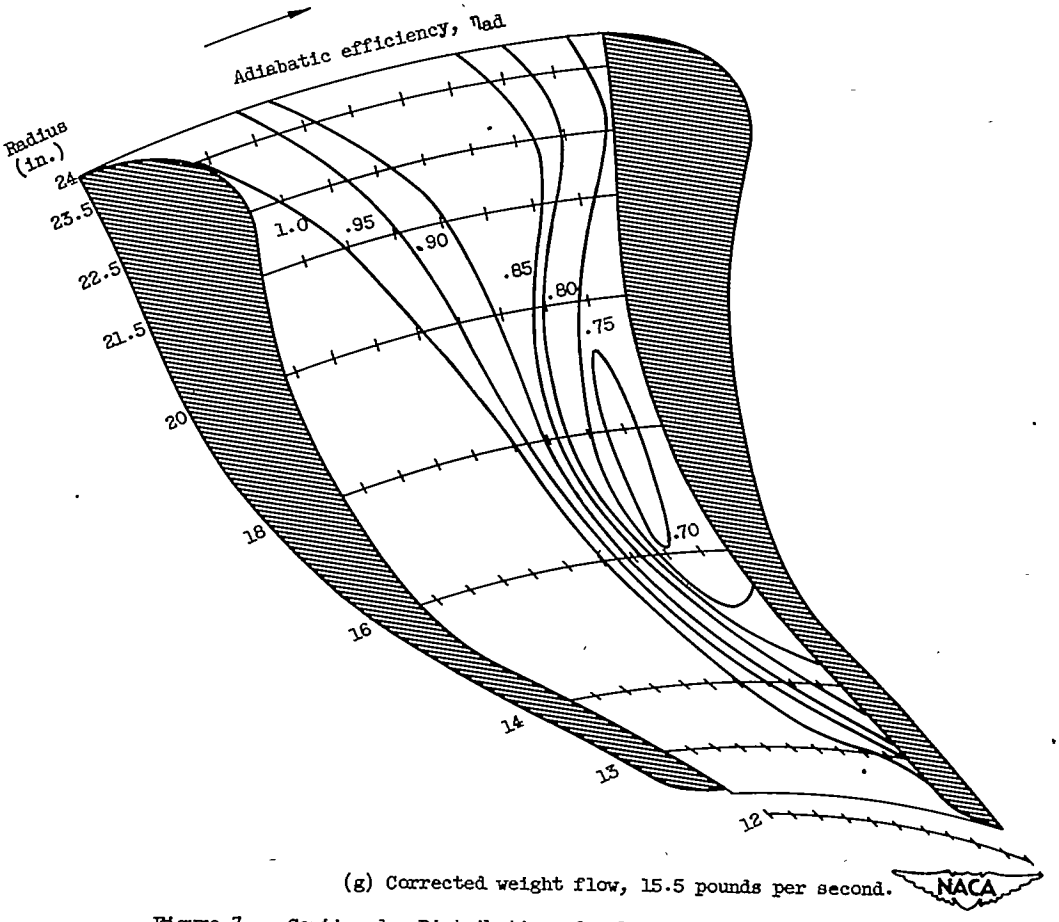

(g) Corrected weight flow, 15.5 pounds per second.

Figure 7. - Continued. Distribution of relative adiabatic efficiency throughout modified impeller passage.

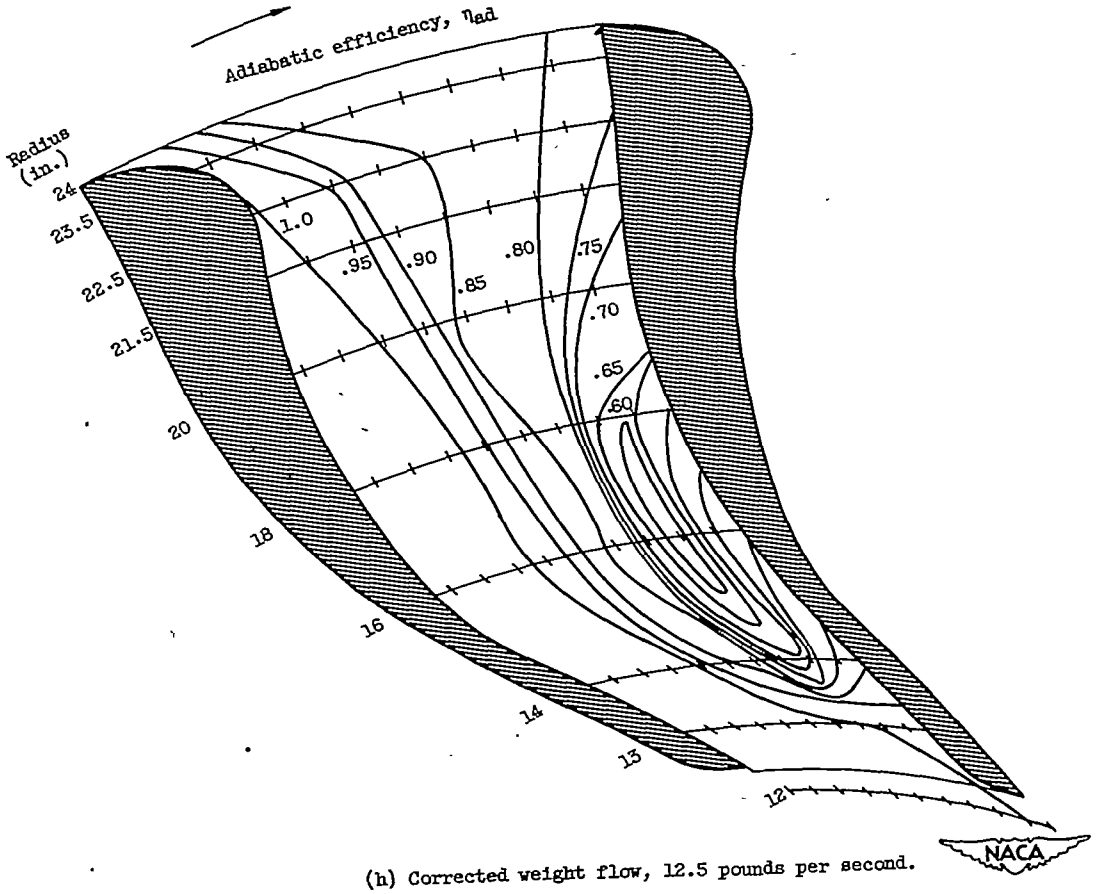

(h) Corrected weight flow, 12.5 pounds per second.

Figure 7. - Continued. Distribution of relative adiabatic efficiency throughout modified impeller passage.

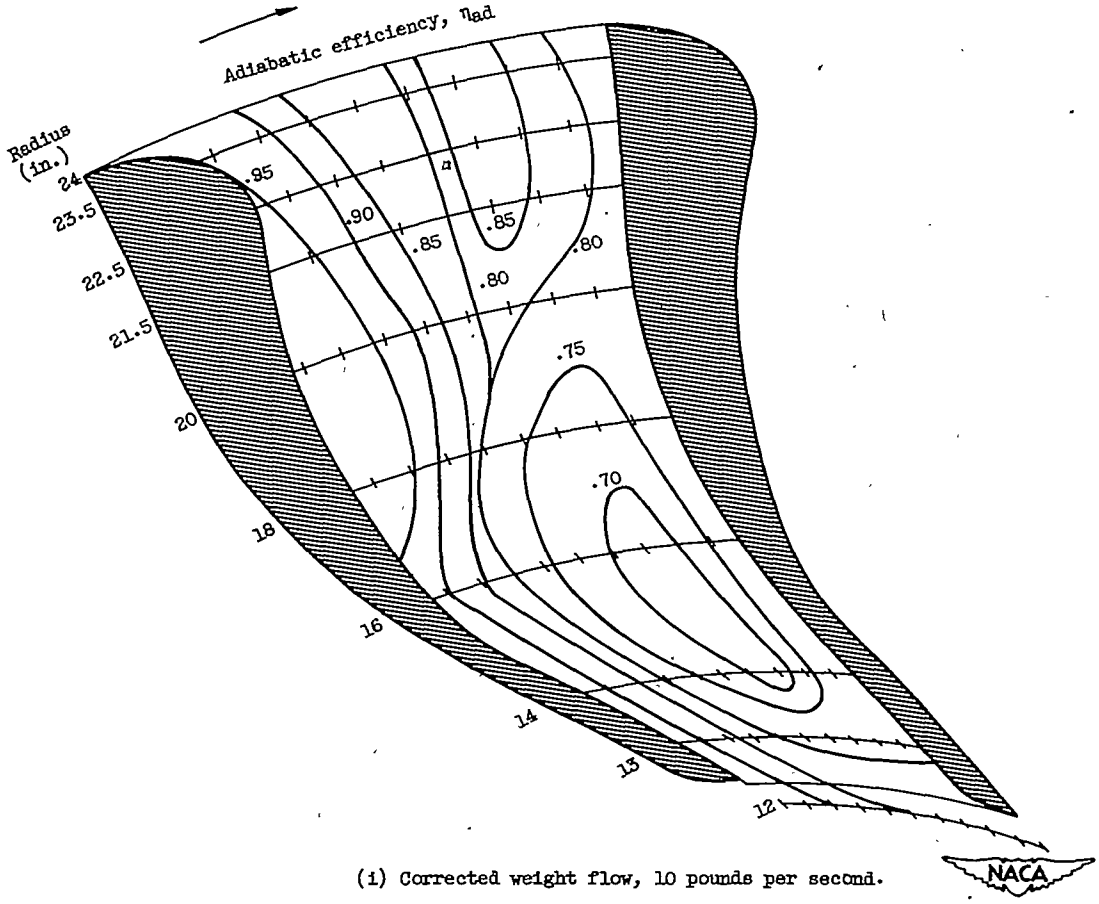

(i) Corrected weight flow, 10 pounds per second.

Figure 7. - Concluded. Distribution of relative adiabatic efficiency throughout modified impeller passage.

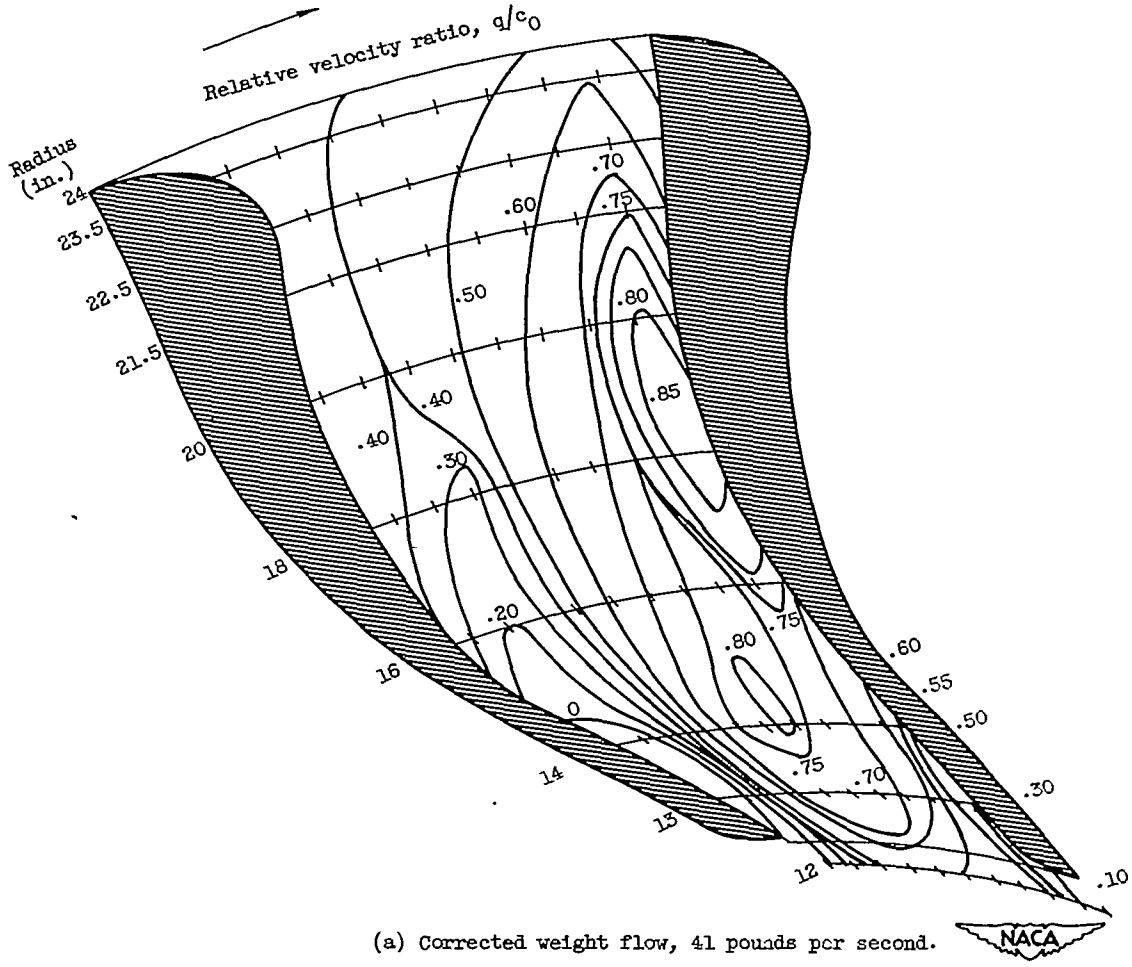

(a) Corrected weight flow, 41 pounds per second.

Figure 8. - Relative velocity ratio distribution throughout modified impeller passage.

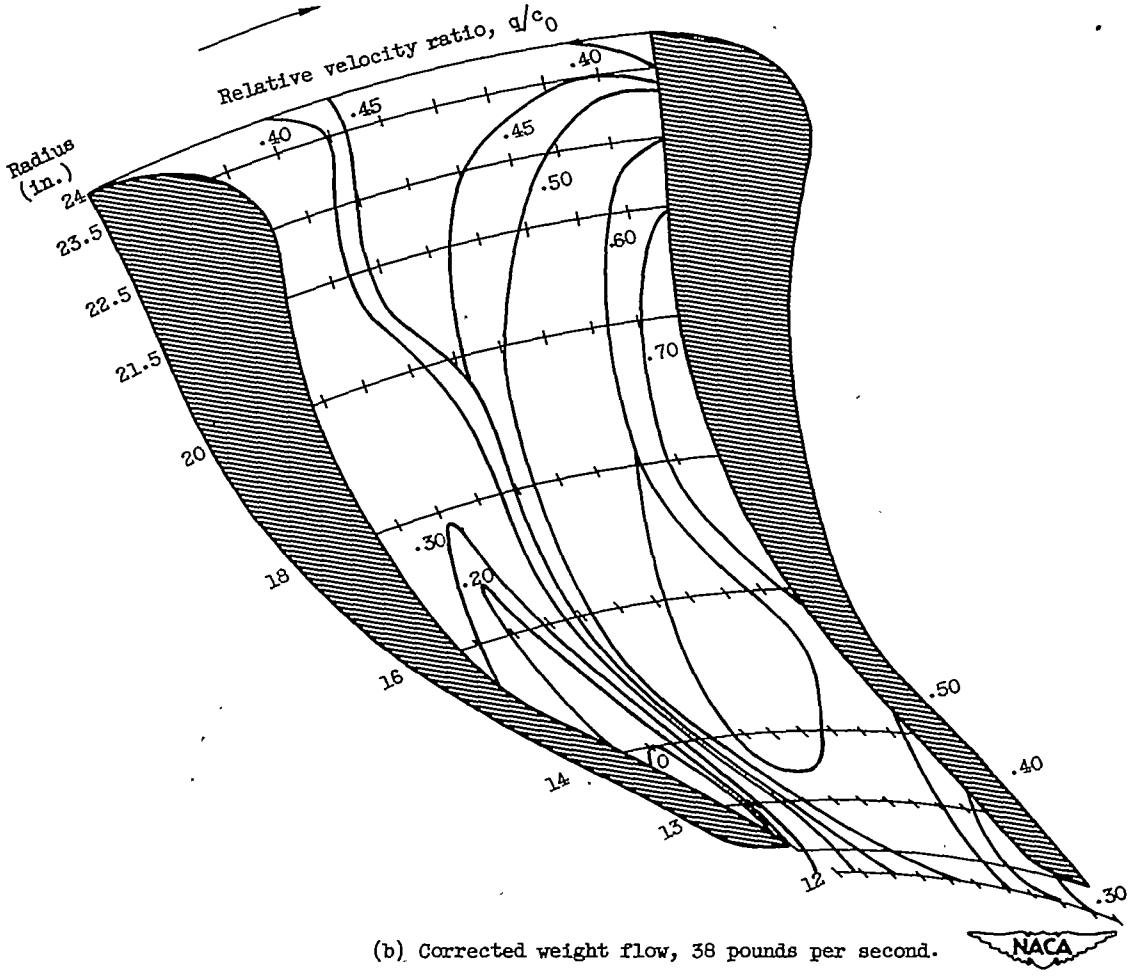

(b) Corrected weight flow, 38 pounds per second.

Figure 8. - Continued. Relative velocity distribution throughout modified impeller passage.

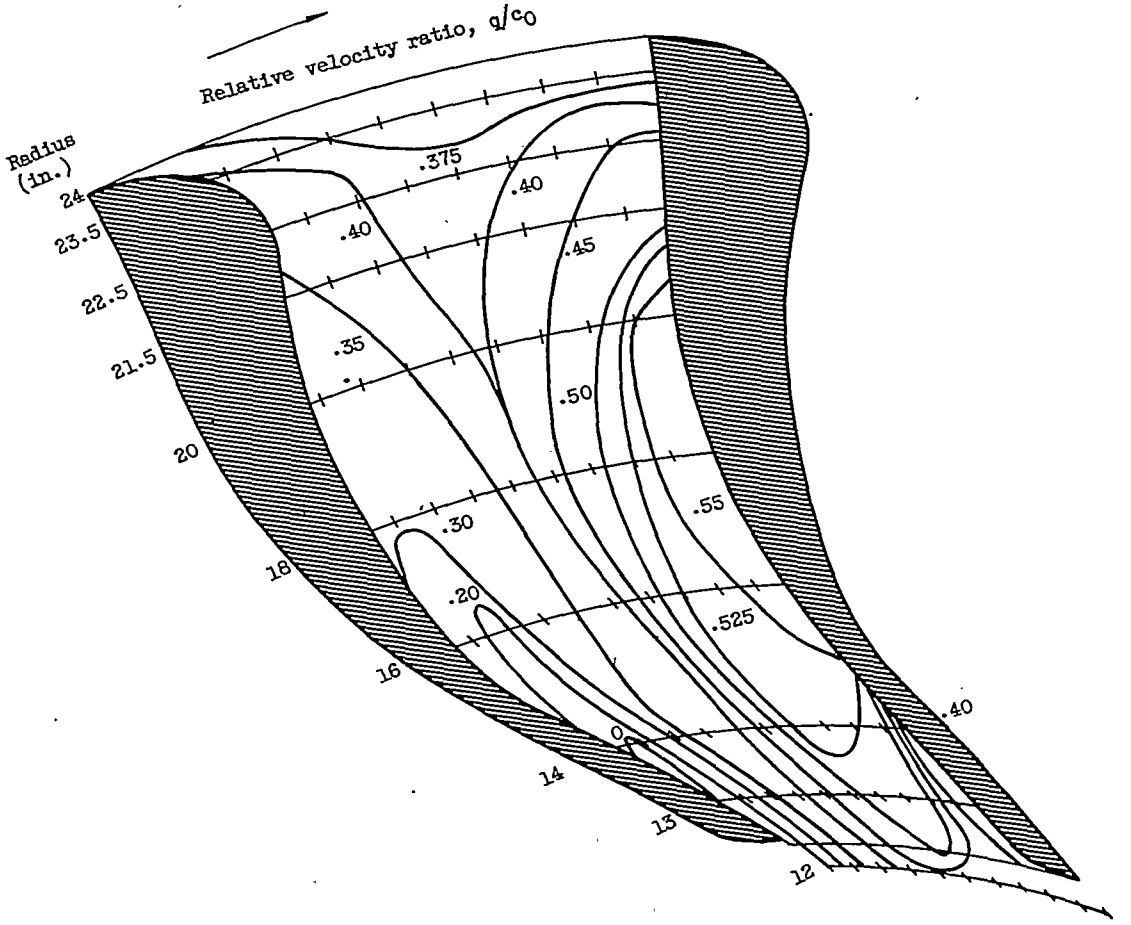

(c) Corrected weight flow, 34 pounds per second.

Figure 8. - Continued. Relative velocity distribution throughout modified impeller passage.

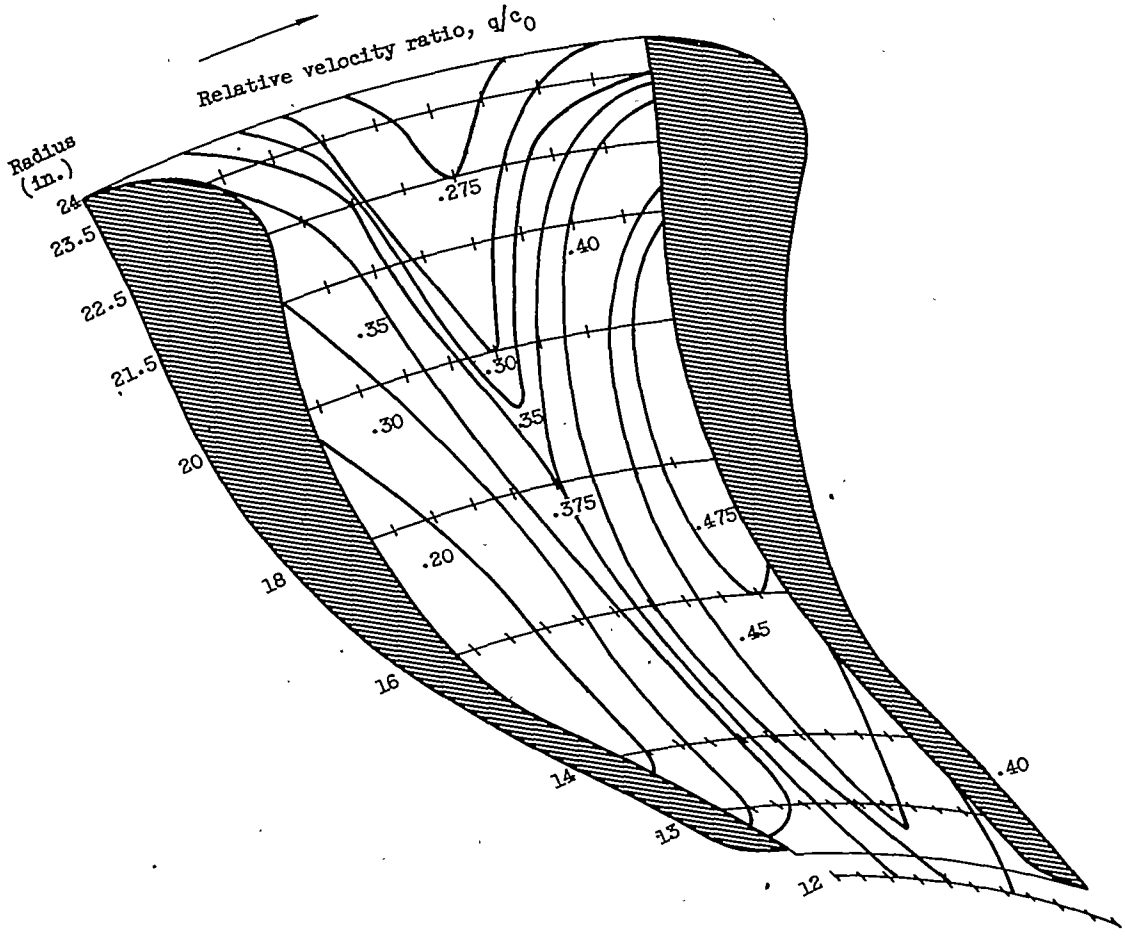

(d) Corrected weight flow, 30 pounds per second.

Figure 8. - Continued. Relative velocity distribution throughout modified impeller passage.

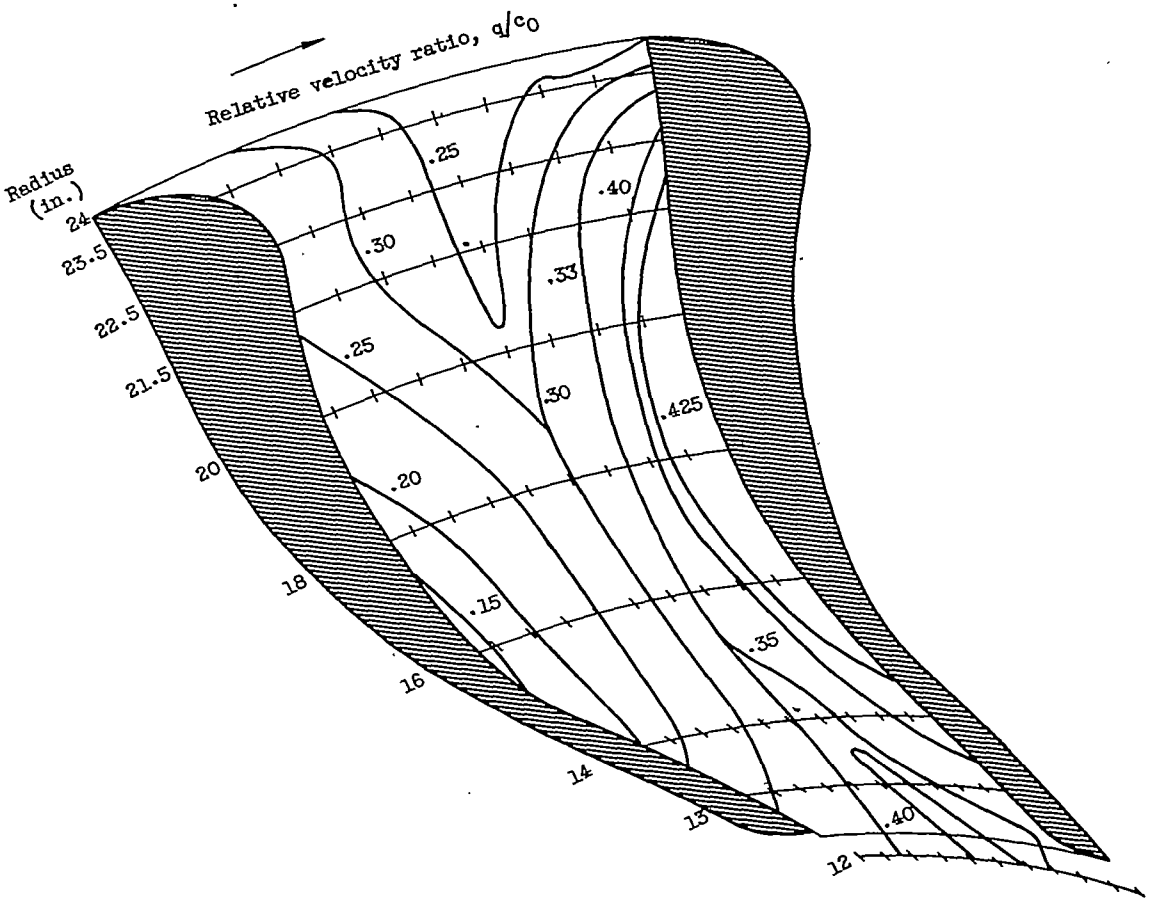

(e) Corrected weight flow, 26 pounds per second.

Figure 8. - Continued. Relative velocity distribution throughout modified impeller passage.

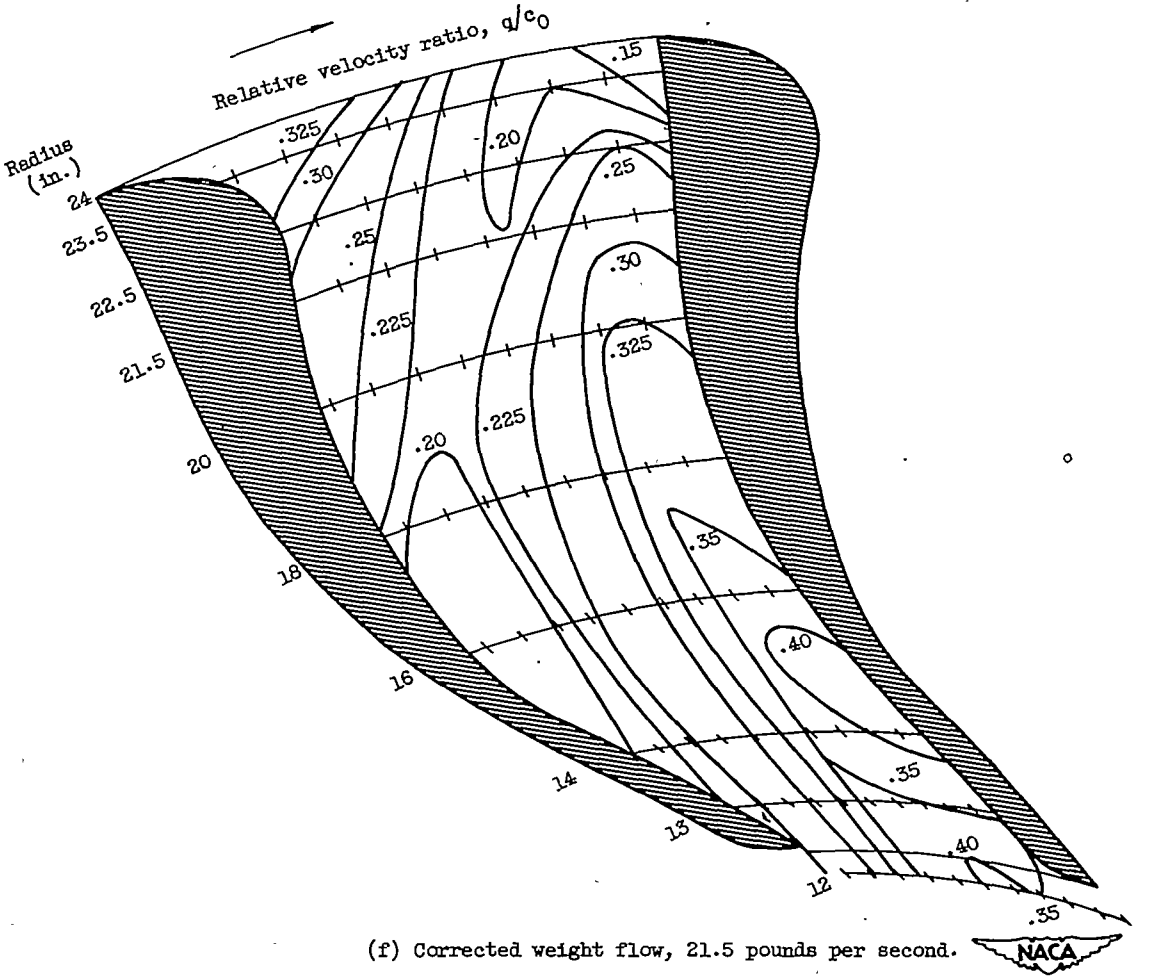

(f) Corrected weight flow, 21.5 pounds per second.

Figure 8. - Continued. - Relative velocity distribution throughout modified impeller passage.

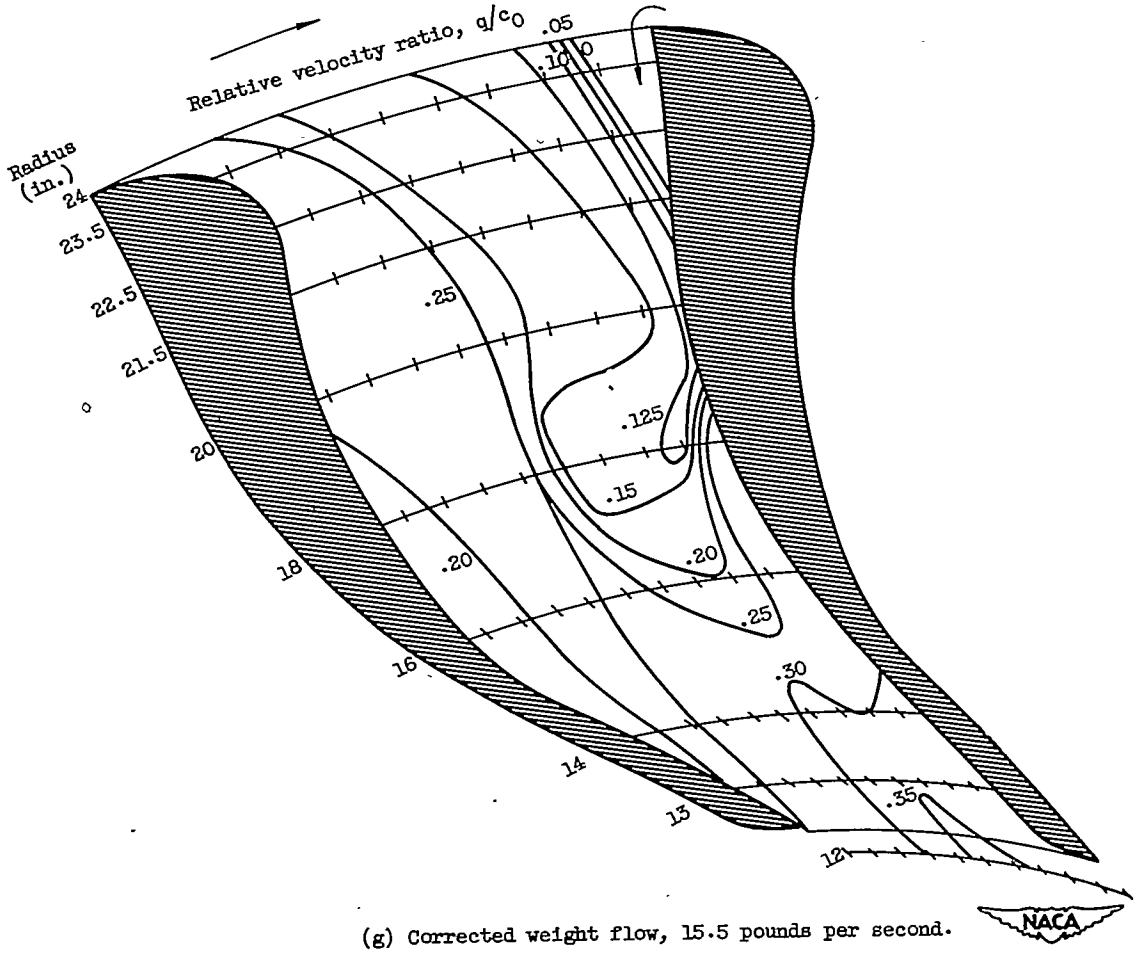

(g) Corrected weight flow, 15.5 pounds per second.

Figure 8. - Continued. Relative velocity distribution throughout modified impeller passage.

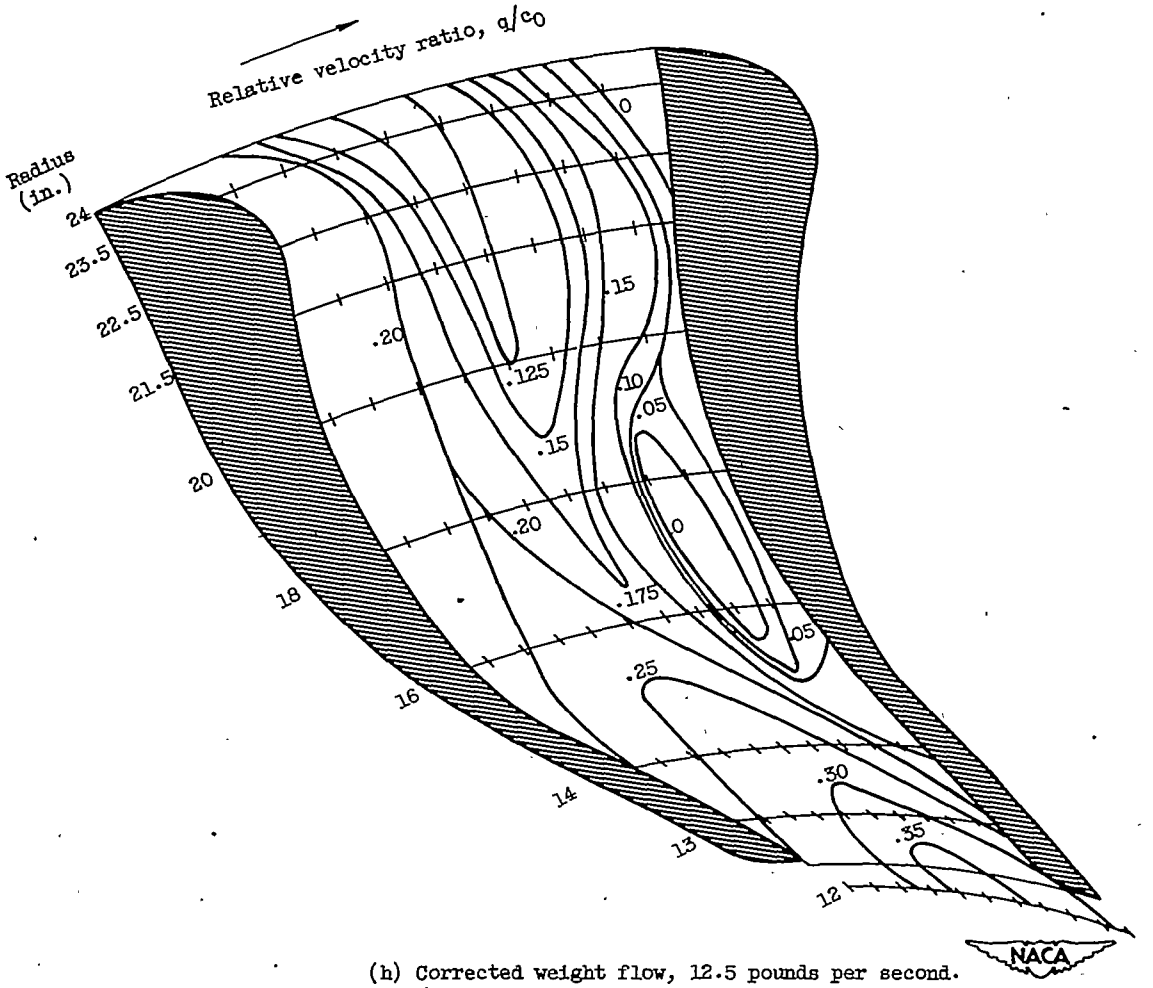

(h) Corrected weight flow, 12.5 pounds per second.

Figure 8. - Continued. Relative velocity distribution throughout modified impeller passage.

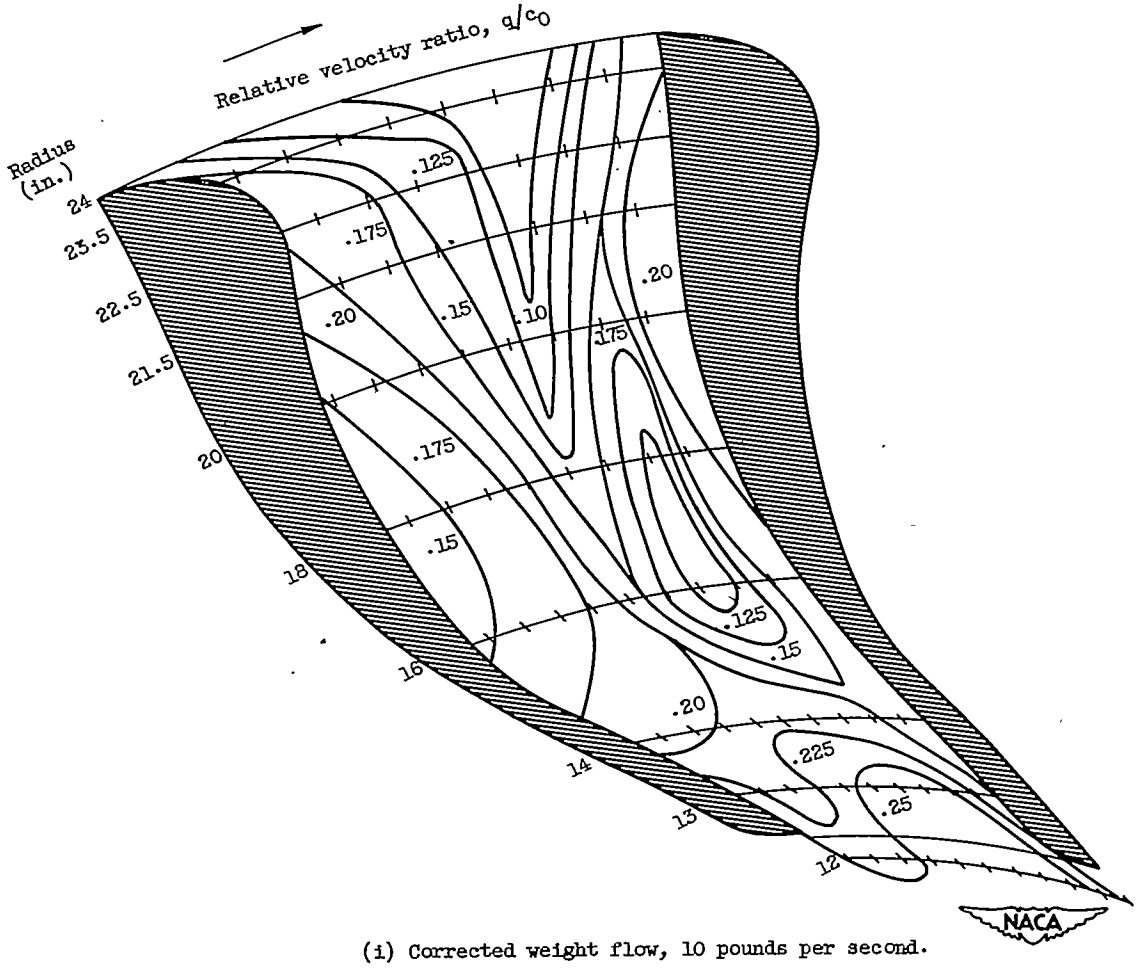

(i) Corrected weight flow, 10 pounds per second.

Figure 8. - Concluded. Relative velocity distribution throughout modified impeller passage.

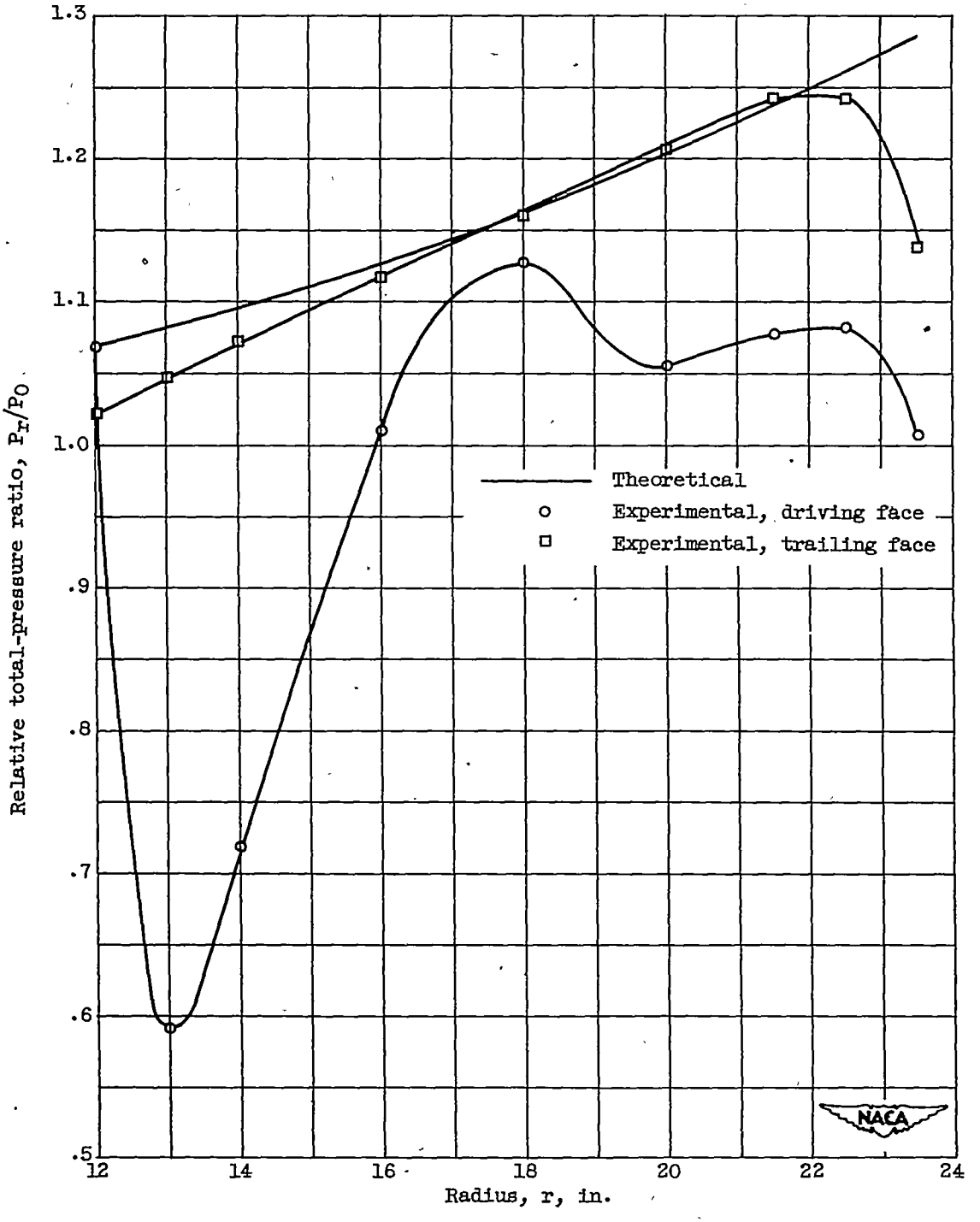

(a) Corrected weight flow, 41 pounds per second.

Figure 9. - Total-pressure distribution near blade surfaces of modified passage at three weight flows.

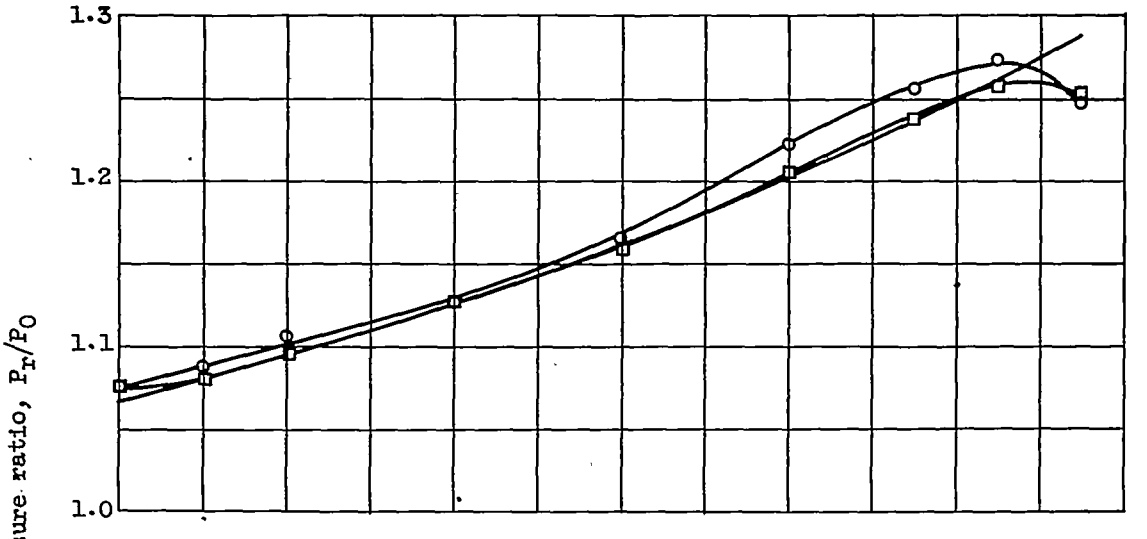

(b) Corrected weight flow, 26 pounds per second.

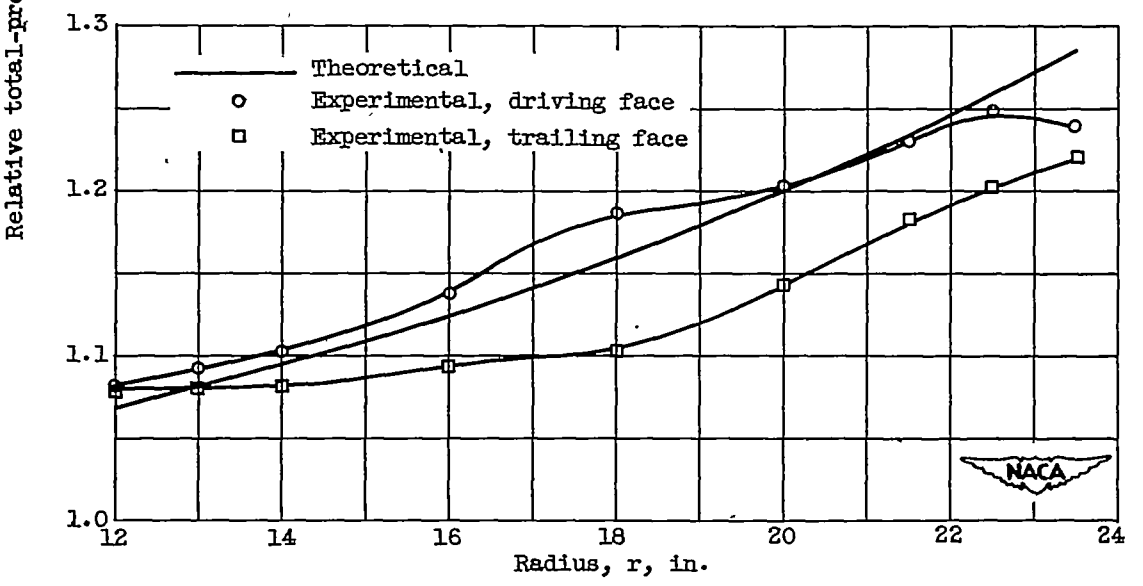

(c) Corrected weight flow, 12.5 pounds per second.

Figure 9. - Concluded. Total-pressure distribution near blade surfaces of modified passage at three weight flows.

NACA-Langley - 5-22-52 - 1000